



Politecnico
di Torino

DENSYS



DAEMONHYC 

Master thesis

To obtain the following master degrees

Master Énergie – Université de Lorraine, France

Laurea Magistrale in Ingegneria Energetica e Nucleare – Politecnico di Torino, Italy

Sustainable Anion Exchange Membrane Electrolyser for large-scale green hydrogen production

Presented by:

José Carlos Martinez Rosales

Supervisors:

Prof. Gaël Maranzana (UL - LEMTA)

Prof. Giuseppe Sdanghi (UL - LEMTA)

Dr. Jérôme Dillet (CNRS – LEMTA)

Prof. Massimo Santarelli (PoliTo)

5 July 2023

Stockholm

Acknowledgements

The master thesis is the last step into obtaining a master's degree. In this case I will be blessed with not only one but two diplomas, from two reputed universities in Europe. These two universities are at the forefront of research in the energy transition, on topics that will define the next decades of human wellbeing, and as such, it is an honour to have been one of their students.

These two years that have elapsed since I travelled abroad to study have been some of the best in my life. I have met wonderful people from all around the world and I have made many great friends as well. This experience has helped me to not only keep looking forward on new exciting personal projects, but to also look backwards, with kindness, to remember what has brought me here to where I stand now.

I would like to thank my father Isaías, who I imagine would be proud of me, and to my mother Sandra who has given me her boundless support. To my aunt and godmother Dilma, who strongly kept encouraging me to look after opportunities like this one, and to my uncle and godfather Santiago, who made sure that I am well dressed for my incoming graduation. And to all my family and friends in Honduras who gave me their support and their best wishes when starting this endeavour back then during the midst of the covid-19 pandemic.

This experience would not have been possible without the economic support from the Erasmus+ programme. Back in June 2021 I received the offer to join the DENSYS programme starting on September 2021, while being entitled to a scholarship for the whole duration of the studies. Once I reached the Charles de Gaulle airport at Paris for the very first time, I finally realized that my life was about to change. I would like to thank the DENSYS programme staff for their hard work and dedication to the realization of this programme that has formed me and to which now I belong.

This master thesis work has been possible thanks to the incredible work and dedication of my supervisors Prof. Gaël Maranzana, Prof. Giuseppe Sdanghi and Dr. Jérôme Dillet at LEMTA. I cannot wait to continue learning with you. Similarly, many thanks to Prof. Massimo Santarelli for his support and guidance throughout this process.

Finally, I would like to thank again Fabrice Lemoine, Heathcliff Demaie and Samira Menouar for the splendid trips to the Vosges. The mountains may become part of my life now. And to my friends and now colleagues Sthefi and Anjali, I don't think I would have enjoyed Italy as much as I did without you.

Abstract

The French national strategy on decarbonized hydrogen aims to install 6.5 GW of electrolyser capacity in France by the year 2030, to develop an industrial sector around hydrogen and to sustain the innovation and research in this sector. For this last reason the French programme PEPR-H2 was created and is operated by the French National Research Agency (ANR). DAEMONHYC is a project lead by the LEMTA and financed by the PEPR-H2 programme that aims to develop new materials and to increase the performance and durability of Anion Exchange Membrane Water Electrolysers (AEMWE).

AEMWE is an emerging technology thanks to the recent advancements in anion exchange membranes that enables the construction of durable zero-gap configuration electrolysers in alkaline environments. This is an improvement over the traditional alkaline water electrolysers (AWE) that have low hydrogen production yields due to the gap between electrodes that brings high internal resistances and therefore lower performances. In this way, AEMWE is similar to the now proven technology of proton exchange membrane water electrolysers (PEMWE), but with the added benefit of not depending on rare and expensive PGM electrocatalysts like Iridium. In fact, Iridium production is so low, reaching only 7 tons annually, that it is considered a potential bottleneck in the deployment of PEMWEs in large scale, and is one reason behind the interest in alternative electrolysis technologies, like AEMWE and SOEC (Solid Oxide Electrolysis Cell).

This master thesis is a firsthand experience into assembling and operating a functional AEMWE cell for the first time at LEMTA, and it aims to provide invaluable guideline for future research in the subject. Two AEMWE cells were assembled using both PGM and non-PGM materials and commercial anion exchange membranes available in the market, and a reference electrode was installed in each cell following the methodology employed at the laboratory. 1 M KOH supporting electrolyte solution was used to supply both water and electrolyte to the cell, and two electrolyte feeding configurations were tested. Polarization curves were obtained for the different configurations and cells at different temperatures—to test the performance of the cells and to obtain electrochemical data for posterior analysis. Finally, a simple electrochemical model was employed to process the data, and the calculated electrochemical parameters are reported.

The results demonstrate how electrolyser performance benefits from higher temperatures, and how anhydrous cathode operation can be advantageous when operating AEMWEs. They also demonstrate the feasibility of operating a PGM-free electrolyser and the gap that still exists in electrocatalyst performance compared to a PGM cell, especially respect to platinum as cathode electrocatalyst for the HER reaction. It is also demonstrated that Iridium is not an outstanding electrocatalyst for the OER reaction in alkaline media. These results are in line with the scientific literature reviewed.

Table of Contents

Acknowledgements	II
Abstract	III
Nomenclature	VI
The laboratory	VIII
Introduction	1
Objectives	3
Literature review	4
Electrolysis technologies.....	4
Catalysts for AEMWE.....	6
Membranes and ionomers for AEMWE.....	10
PAP: Poly (aryl piperidinium).....	10
PNB: Poly (norbornene).....	12
Other AEM membranes.....	13
Interaction of materials and system configuration	14
Methodology	18
Anion Exchange Membrane Water Electrolysis Cell.....	18
Experimental setup.....	19
AEMWE characterization	21
Electrode potentials	21
Procedure for calculating the electrode potentials from reference electrode data	23
Results, analysis and discussion.....	26
Performance of the cells	26
Performance of the components	29
Conclusions	32
Perspectives	33
References	34
Appendix	42

List of Figures

Figure 1. DAEMONHYC Project and its partners, adapted from (“DAEMONHYC,” n.d.).....	VIII
Figure 2. Representation of the five main types of water electrolyzers (Chatenet et al., 2022).....	4
Figure 3. Schematic representation of the AEMWE (Vinodh et al., 2023).....	5
Figure 4. Protocol for measuring the electrochemically active surface area, catalytic activity, stability and Faradaic efficiency of heterogeneous electrocatalysts for OER (McCrorry et al., 2013).....	7
Figure 5. Chemical structure of PiperION TP-85 membrane (Endrődi et al., 2020).....	10

Figure 6. Influence of temperature on a pure water-fed electrolyser with PiperIon 50 μm MEA (Lindquist et al., 2021)	10
Figure 7. Chemical structures of Pention and of crosslinked PNB polymer (Z. Wang et al., 2023), (N. Shah et al., 2023).....	12
Figure 8. Illustration of ion-transport pathways of a half cell (anode) when DI water and KOH solutions are fed to the AEM electrolyzers (Liu et al., 2021).....	15
Figure 9. (a) Water content and reaction current density distribution in the cCL. (b) Water vapor partial pressure in the cCL and cPTL at 0.5 A/cm ² for cells with different cCL HEI properties (Liu & Weber, 2022).....	16
Figure 10. AEMWE cell performance comparison at 60 °C using 1 M KHCO ₃ and 1 M KOH as feedstock (L. Wang et al., 2019)	16
Figure 11. Pourbaix diagrams of cobalt, copper, iron, and nickel in aqueous electrolytes at ambient pressure and 25 °C (Du et al., 2022)	17
Figure 12. Diagram of an AEMWE Cell, adapted from (Zheng et al., 2018)	18
Figure 13. Experimental setup.....	19
Figure 14. PiperIon (a) and Pention (b) AEMs	19
Figure 15. Endplates (a) and PTLs (b) showing both sides.....	20
Figure 16. Cell configurations used during the experiments.....	20
Figure 17. Representation of electrode potentials in PEM water electrolysis in presence of current (Parra-Restrepo, 2020)	22
Figure 18. Numerically resolved potential distribution in the three phases and isopotential lines for the case of perfect alignment of the two electrodes (Cazot, 2019)	23
Figure 19. (a) Illustration of ohmic region and kinetic region for an AEMWE cell (b) example of deduced electrode potentials for the same cell.....	24
Figure 20. Corrected electrode potentials versus the Butler-Volmer model for each electrode. Example is for a cell operating at 60 °C.....	25
Figure 21. Example of results from minimizing the sse for a data set obtained at 61 °C	25
Figure 22. Polarization curves of the cell # 1 at different temperatures.....	26
Figure 23. Performance comparison between cell # 1 (anode fed) and cell # 2 (cathode fed).....	27
Figure 24. Performance comparison between cell #1 (GDE) and cell # 3 (CCM).....	27
Figure 25. Efficiency comparison between cell #1 (GDE) and cell # 3 (CCM)	28
Figure 26. Comparison of (a) Area specific resistances and (b) estimated exchange current densities between cell #1 and #3	30
Figure 27. Comparison of (a) measured polarization curve versus electrochemical model and of (b) electrode overvoltage and Butler-Volmer model for cell #3.....	30

List of Tables

Table 1. Performance of several catalysts used in OER under alkaline media	8
Table 2. Performance of several catalysts used in HER under alkaline media	9
Table 3. Performance of AEMWE cells using PAP polymers	11
Table 4. Performance of AEMWE cells using PNB polymers.....	12
Table 5. Performance of AEMWE cells using other membranes.....	13
Table 6. Performance of AEMWE cells tested in this work	28
Table 7. Results from parameter fitting in MATLAB.....	29
Table 8. Estimated performance of HER catalysts used in this work	31
Table 9. Estimated performance of OER catalysts used in this work	31

Nomenclature

Abbreviation	Definition
AEI	Anion Exchange Ionomer
AEM	Anion Exchange Membrane
AEMWE	Anion Exchange Membrane Water Electrolyser
ANR	Agence National de la Recherche
ASR,	Area Specific Resistance
AWE	Alkaline Water Electrolyser
BP	Biphenyl Pepsiridinium
CCM	Catalyst Coated Membrane
CCS	Catalyst Coated Substrate
CCUS	Carbon Capture Utilisation and Storage
CF	Compensation Factor
CL	Catalyst Layer
CNRS	Centre National de la Recherche Scientifique
CNT	Carbon Nanotubes
DAEMONHYC	Durable Anion Exchange Membrane electrOlyser for large-scale green Hydrogen produCtion
DENSYS	Decentralised Smart Energy Systems
DI	Deionized water
ECSA	Electrochemical Active Surface Area
FC	Fuel Cell
GDE	Gas Diffusion Electrode
GDL	Gas Diffusion Layer
GHG	Greenhouse Gases
HEI	Hydroxide Exchange Ionomer
HEM	Hydroxide Exchange Membrane
HEMWE	Hydroxide Exchange Membrane Water Electrolyser
HER	Hydrogen Evolution Reaction
HFR	High Frequency Resistance
IEA	International Energy Agency
IEC	Ion Exchange Capacity
LEMTA	Laboratoire Énergies et Mécanique Théorique et Appliquée
MEA	Membrane Electrode Assembly
MPL	Microporous Layer
NF	Nickel Foam
NM	Nickel Mesh
OER	Oxygen Evolution Reaction
PAP	Poly (Aryl Pepsiridinium)
PBP	Poly (Biphenyl Pepsiridinium)
PCCEL	Proton Conducting Ceramic Electrolyser
PEM	Proton Exchange Membrane
PEMWE	Proton Exchange Membrane Water Electrolyser
PEPR	Programme et Equipements Prioritaires de Recherche

PGM	Platinum Group Metal
PNB	Poly (Norbornene)
PTFE	Polytetrafluoroethylene
PTL	Porous Transport Layer
RDS	Rate Determining Step
RH	Relative Humidity
RHE	Reversible Hydrogen Electrode
SCL	Surface Catalyst Layer
SHE	Standard Hydrogen Electrode
SOEC	Solid Oxide Electrolysis Cell
SS	Stainless Steel
TP	Terphenyl
TPB	Triple Phase Boundary
TS	Tafel Slope
UL	Université de Lorraine
UNFCCC	United Nations Framework Convention on Climate Change

Symbol	Definition	Unit
j_0, i_0	Exchange current density	[A cm ⁻²]
η	Overvoltage	[V]
α	Electron transfer coefficient	[-]
λ	Equilibrium water content	[-]
σ	Ionic conductivity	[mS/cm]
ϕ^m	Potential of metallic phase of the electrode	[V]
ϕ^e	Potential of electrolyte surrounding the electrode	[V]
U_{cell}	Difference of potential across the cell	[V]

Constant	Definition	Value
R	Ideal gas constant	8.314 J (mol K) ⁻¹
F	Faraday constant	96485 C mol ⁻¹

The laboratory

LEMTA (*Laboratoire Énergies & Mécanique Théorique et Appliquée*) is a research laboratory of the University of Lorraine (UL) and the CNRS (*Centre National de la Recherche Scientifique*). It is attached to the scientific center EMPP (*Énergie Mécanique Procédés Produits*) of the UL and to INSIS (*Institut des sciences de l'ingénierie et des systèmes*) of CNRS (Moine, 2023).

Some key words that summarize the competences and know-how of the laboratory includes porous media, multiphase flow, rheology, electrochemical systems, thermal metrology, acoustics, laser metrology, NMR, soil mechanics, powders and suspensions, micro and nano scales, numeric simulation and artificial intelligence, nuclear safety, fire control, etc. All these are associated with multi-physic approaches at different scales, from matter to energy systems (Moine, 2023).

The laboratory recently celebrated its 50th anniversary since its creation in 1973 and by the time of writing this thesis it groups around 190 collaborators including researchers, doctoral and postdoctoral staff, and personnel that supports its research (Moine, 2023). The laboratory participates in projects of the PEPR (*Programme et Equipements Prioritaires de Recherche*) including the DAEMONHYC project, which aims to develop the materials that will be used in the next generation of AEMWEs (“DAEMONHYC,” n.d.). The laboratory has more than twenty years of experience with electrochemical systems, ranging from PEM Fuel Cells up to its latest addition, AEM Water Electrolysis, as it can be appreciated in Figure 1.



Figure 1. DAEMONHYC Project and its partners, adapted from (“DAEMONHYC,” n.d.)

Introduction

The last centuries have been marked by an impressive technological development that has raised human living conditions to really high standards. This development has been unequal and some countries have benefited more from it than others. In recent decades there has been an increasing awareness in improving life standards for all human population, an example of this was the United Nations millennium development goals which were superseded by the Sustainable Development Goals from the year 2015 (*United Nations Millennium Development Goals*, n.d.).

In a similar way, the last decades have seen increasing environmental awareness. The Montreal Protocol established in the year 1987 resulted in the successful regulation of Ozone Depleting Substances, and helped in the recovering of the Ozone layer, saving millions of lives (*About Montreal Protocol*, 2018). In the year 1992 it was adopted the United Nations Framework Convention on Climate Change (UNFCCC) as a response to the undeniable effects of human activities on the climate system (*About the Secretariat | UNFCCC*, n.d.). The Kyoto Protocol of 1997 and the Paris Agreement of 2015 are the result of UNFCCC's efforts to stabilize Greenhouse Gases Emissions (GHG).

The Paris Agreement in particular aims to maintain the rise of global temperature to 1.5 °C by the end of the century respect to pre-industrial levels (*The Paris Agreement | UNFCCC*, n.d.). Reaching Net-zero CO₂ emissions by 2050 is consistent with the objectives of the Paris Agreement and it has been chosen as a target by governments and international organizations like the International Energy Agency (IEA) (*Net Zero by 2050 – Analysis*, n.d.). Achieving so requires action across the whole energy system, and for some hard-to-abate sectors low emissions hydrogen is the only decarbonisation solution (*World Energy Transitions Outlook 1-5C Pathway 2022 Edition*, 2022).

Low emissions hydrogen is now being produced predominantly from fossil fuels plants equipped with carbon capture, utilisation and storage (CCUS) (*Global Hydrogen Review 2022 – Analysis*, n.d.). Hydrogen produced via electrolysis with renewable energies or green hydrogen is gaining importance and by 2030 the expected installed electrolyser capacity is estimated around 200 GW if all the current projects are realised (*Global Hydrogen Review 2022 – Analysis*, n.d.). This however still falls short to the 860 GW of electrolyser capacity expected by the year 2030 if we were to follow a path compatible to reaching zero emissions by 2050 (*Net Zero by 2050 – Analysis*, n.d.). The IEA expects the electrolyser capacity to ramp up to 3600 GW by 2050.

The French government was one of the first to realize the potential of hydrogen, and is doing a big investment in the sector with the goal of achieving technological development and foster the ecological transition (Pompili & Le Maire, 2020). The French national strategy on decarbonized hydrogen targets to deploy 6.5 GW of electrolyser capacity in France by the year 2030, to develop an industrial sector around hydrogen and to sustain the innovation and research in this sector. For this last point, the French National Research Agency (ANR) is operating the

Programme et Equipments Prioritaires de Recherche sur l'hydrogène décarboné (PEPR-H2) with the goal to prepare the next generation of hydrogen technologies.

One recent article from *Chemical and Engineering News* (2023) explores the 4 main electrolyser technologies that are used or under development: Alkaline water electrolysis is the most widespread technology due to its robustness and lower costs. PEM electrolyzers though somewhat more expensive than alkaline electrolyzers are preferred in applications that require flexible size and throughput, and research is oriented into how to decrease the amounts of iridium and platinum in the electrodes. Solid Oxide Electrolyzers operate at high temperatures of 600-900 °C, allowing this technology to approach 100% efficiency if used simultaneously with waste heat from other sources. Finally, AEM electrolyzers combine using a polymeric material like PEM electrolyzers while using alkaline conductors that allows the use of non-precious metal catalysts. This combination makes it the holy grail of electrolyser technologies (*Electrolyzers*, 2023).

This thesis focuses on the technology of Anion Exchange Membrane Water Electrolysis (AEMWE). This is the latest venture of LEMTA in the frame of the DAEMONHYC Project. This project is a collaboration of 5 French research laboratories and 2 industrial partners with experience in the sector. The project is funded by the PEPR-H2 and it aims to improve the durability and performance of AEM water electrolyzers by developing new ionomers and materials based on non-precious metal catalysts.

LEMTA has more than 20 years of experience in hydrogen technologies, but this is its first attempt at operating an AEMWE cell. This work is then a first contact point with the technology and will provide invaluable experience that will serve as basis for future work to come.

Objectives

- ✚ Set up a new experimental bench to operate and characterize an Anion Exchange Membrane Water Electrolysis cell.
- ✚ Benchmark the different electrodes and membranes available on the market.
- ✚ Model the mass, heat and charge transfer phenomena.

Literature review

Electrolysis technologies

The 2022 Global Hydrogen Review of the IEA (*Global Hydrogen Review 2022 – Analysis*, n.d.) provides valuable insights into the global hydrogen situation: For the year 2020, water electrolysis accounted for 0.03% of hydrogen production for energy and chemical feedstocks; of the installed global electrolyser capacity more than 40% is based in Europe; and of the installed capacity, alkaline electrolysers dominates with 61% of the installed capacity, followed by PEM with 31%, and the remaining capacity being supplied by SOEC and other unspecified technologies. From the IEA’s review we can also obtain a glimpse of the price targets for green hydrogen: By 2030 the price of green hydrogen is expected to fall as low as 1.3 USD per kg and to continue falling to 1 USD per kg long term in the Net-Zero Emissions scenario, making the price competitive with hydrogen from natural gas even without CCUS. As the IEA’s review points out, reaching this point from current prices of 3 to 8 USD per kg will depend on many factors including cheaper renewable energy and technological improvements in electrolysis and other auxiliary equipment.

Figure 2 illustrates the main types of electrolysers and allows to compare their differences and similarities. As it was mentioned previously, AWE is the most robust and widespread electrolyser technology, and is characterized by the usage of a porous diaphragm that enables ionic contact between the electrodes and impedes the intermixing of the produced gases (Aili et al., 2023). One of the advantages of AWE is the alkali metal hydroxide aqueous electrolyte, which enables using non-PGM catalysts, while its drawbacks includes the effect of gas bubbles in the conductivity of the electrolyte, the possible intermixing of gases, and that it cannot be operated in transient regime making their coupling to renewables awkward (Chatenet et al., 2022).

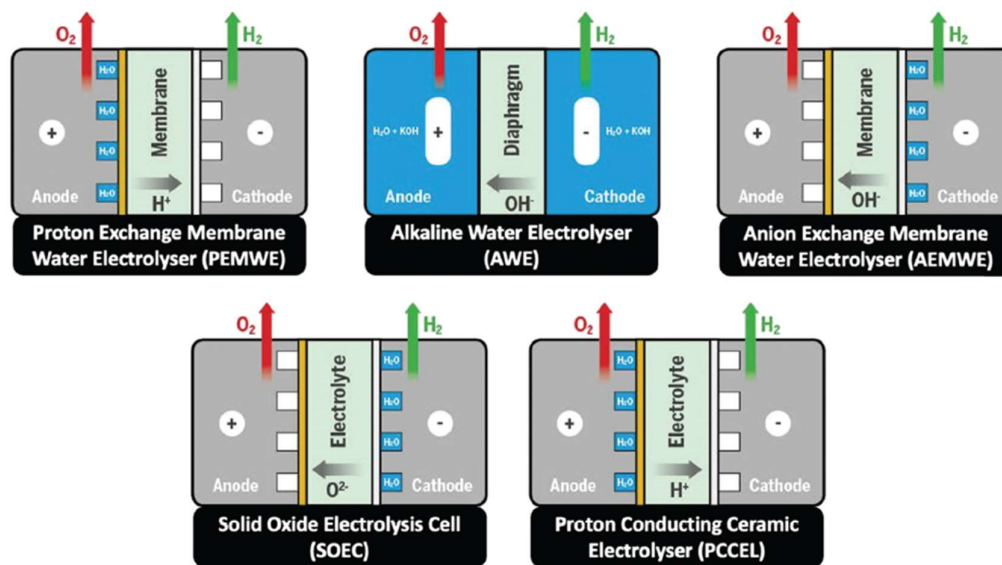


Figure 2. Representation of the five main types of water electrolysers (Chatenet et al., 2022)

PEM water electrolysis is the most effective water electrolysis technology, and is characterized by the use of proton-conducting polymer electrolyte (e.g. Nafion[®]) that is sandwiched between an anode and a cathode (Chatenet et al., 2022). As Chatenet et al describe in their review, the main advantages of PEMWE over other water electrolyzers are the possibility to operate at high current densities, high efficiencies, high purity of generated gases and a high dynamic range which facilitates its integration with renewable energy sources. In PEMWE the oxygen evolution reaction (OER) at the anode is sluggish and Ruthenium and Iridium oxides are considered the benchmark catalyst with the optimal adsorption energies for O* (Fu et al., 2023). Fu et al in their article explain that RuO₂ despite having better OER activity it is unstable, hence, Ir-based catalysts are considered the only candidates because of their outstanding balance between catalytic activity and stability. Iridium production rates are only around 7 tons per year, and its demand for PEMWE will represent a potential bottleneck in the realization of a mature market of this technology (Minke et al., 2021).

Current research in PEMWE aims to decrease the amounts of PGM metals like Ir used as catalyst, but this also opens the door to emerging electrolysis technologies that do not require expensive PGM materials to operate. In the case of AWE, it is possible to use a non-porous membrane with high anionic conductivity and porous catalyst layers (CL) on each side of the polymeric membrane to form a membrane electrode assembly (MEA) analogous to how PEMWE cells are constructed, with the benefit of decreasing the internal resistance of the electrolyser and allowing the operation of the cell at higher pressures (Chatenet et al., 2022). As Chatenet et al points out, the alkaline environment allows a great variety of catalyst which could permit the use of non-precious metals for the hydrogen and oxygen evolution reactions. Compared to conventional AWE, AEMWE based on anion exchange membranes (AEM) has the potential to become one of the most promising electrolysis systems thanks to the possibility of using inexpensive materials (Hua et al., 2023).

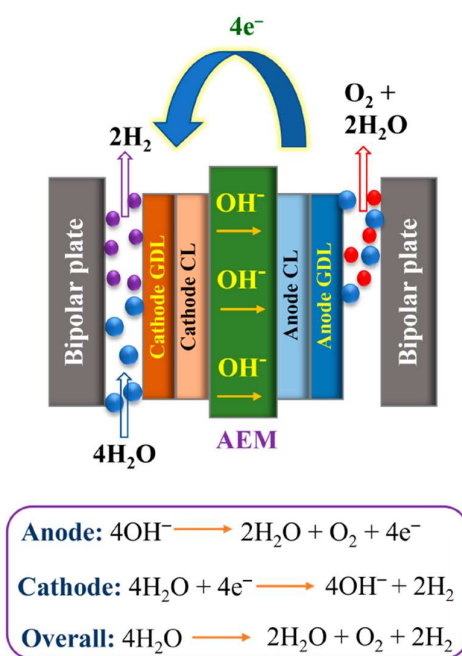


Figure 3. Schematic representation of the AEMWE (Vinodh et al., 2023)

Figure 3 shows a schematic representation of an AEMWE cell: The main constituents include an anion exchange membrane, gas diffusion layers (GDL), electrocatalysts in catalyst layers (CL), and current collectors. The theoretical reversible voltage under typical environment is 1.23 V as determined by the free Gibbs energy of water splitting, however, in general, the working voltages of AEMWE devices are very high primarily due to kinetic energy and iR drop (Vinodh et al., 2023). The membrane electrode assembly (MEA) is the core component in AEMWE devices, which consist of catalyst layer (CL) and membrane, and generally there are two different fabrication methods: Catalyst-coated substrate (CCS) where the catalyst ink is directly deposited on the GDL to form a CL, and catalyst-coated membrane (CCM) where the CL is formed by coating catalyst ink on the membrane (Hua et al., 2023).

The last two technologies that Chatenet et al mention in their review are solid oxide electrolyser cell (SOEC) and proton conducting ceramic electrolyser (PCCEL). Both operate at higher temperatures enabling superior efficiency compared to low temperature electrolyzers but suffer from poor thermo-mechanical properties (Chatenet et al., 2022). SOEC not only can produce pure hydrogen from the direct electrolysis of water but it also can co-electrolyze mixtures of water and CO_2 to produce syngas, which can in turn be utilized to synthesize a variety of hydrocarbons (Javed et al., 2022).

Catalysts for AEMWE

The exchange current density J_0 and the current measured at a specific overvoltage η are indicators of the activity of a catalyst and are often presented as mass activity (current per catalyst mass) or intrinsic activity (current per ECSA, electrochemical surface area) (Du et al., 2022). The Tafel equation (1) reflects kinetic information and yields the Tafel slope value b which gives reaction mechanistic information; to be valid the Tafel slope needs to be determined at a η value exceeding RT/F , typically higher than at least 45-50 mV (Du et al., 2022). As Du et al explain, by extrapolating a Tafel plot to a η value of 0 it yields J_0 , and that the highest Tafel slope value measurable is 120 mV/dec (at 20 °C) since higher slopes indicate that other electrochemical phenomena might be involved.

$$\eta = a + b \log j \quad (1)$$

Du et al also add that only steady state measurements should be used when determining Tafel slope, and that non steady state methods should be avoided. Anantharaj et al (2021) explain that the Tafel slope is highly dependent on the surface coverage θ , which is generally assumed to be either 0 or 1 depending on the rate determining step (RDS) and only when the interface is in a steady state.

Another factor that can affect the determination of the Tafel slope is the iR drop or ohmic drop. In three electrode systems the major contributors for this potential drop are the electrolytic conductivity and the distance between the reference electrode (RE) and the working electrode (WE) (Anantharaj & Noda, 2022). As Anantharaj et al explain, in electrochemistry diagnosis

avoiding completely the iR drop is impossible and it must be corrected to present the intrinsic activity of the catalyst and to use the polarization curve for Tafel analysis.

In the most rudimentary form, overvoltage's associated with the electrode kinetics can be related to the current density at an electrode by the Butler-Volmer equation (2) (Chatenet et al., 2022):

$$j = j_0 \left[\exp\left(\frac{\alpha F}{RT} \eta\right) - \exp\left(\frac{-(1-\alpha)F}{RT} \eta\right) \right] \quad (2)$$

The multistep character of reactions of interest in water electrolysis are hidden in two effective parameters, the effective exchange current density $j_{0,eff}^a$ and the effective transfer coefficient, α_{eff}^a —For this latter parameter, the Tafel slope can be introduced as $b = RT/\alpha_{eff}^a F$ (Chatenet et al., 2022).

Many aspects are evaluated when researchers study electrocatalysts: Figure 4 illustrates a protocol used for measuring several properties of heterogenous electrocatalysts for OER, including ECSA, catalytic activity, stability, and faradaic efficiency.

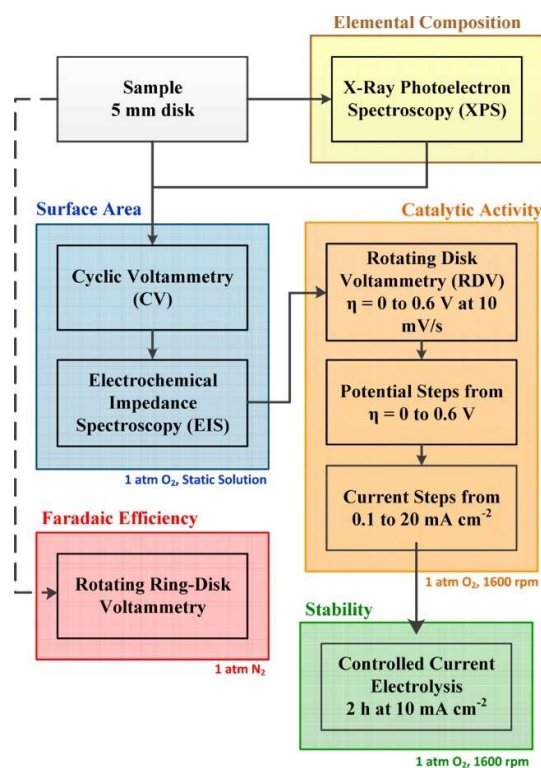


Figure 4. Protocol for measuring the electrochemically active surface area, catalytic activity, stability and Faradaic efficiency of heterogeneous electrocatalysts for OER (McCrory et al., 2013)

Electrocatalysts are also evaluated in acidic or alkaline environments. In their study, McCrory et al (2013) found that IrOx was the only catalyst tested stable under acidic conditions as every non-noble metal catalyst investigated was unstable under oxidative conditions in 1 M H₂SO₄. In contrast, in 1 M NaOH every non-noble metal catalyst investigated achieved 10 mA/cm² at

overpotentials between 0.35 and 0.43 V. Tahir et al (2017) in their review conclude that there are some catalysts that have very good OER activity (<300 mV @ 10 mA/cm²), much better than noble metal catalysts in alkaline medium, but currently most of the OER electrocatalysts function only under alkaline conditions.

This higher stability of OER catalysts in alkaline conditions is one of the advantages that AEM water electrolysis has over PEMWE, which has remained restrained to use Ir-based catalysts. This has opened the door to the development of a huge variety of catalysts which has comparable if not better performance to iridium in alkaline media as shown in Table 1.

Table 1. Performance of several catalysts used in OER under alkaline media

Catalyst (OER)	Electrolyte	η (mV) at j mA/cm ²	TS (mV/dec)	Ref
Ni ₂ P/Ni ₇ S ₆	1.0 M KOH	257 mV @ 100 mA/cm ²	69	(F.-L. Wang et al., 2023)
Ni ₃ C/C	1 M KOH	316 mV @ 10 mA/cm ²	46	(Xu et al., 2016)
NiO	1 M KOH	470 mV @ 10 mA/cm ²	85	(Xu et al., 2016)
316SS CCE-10h	1 M KOH	254 mV @ 10 mA/cm ² (20 °C)	41	(Todoroki & Wadayama, 2019)
IrO ₂	1 M KOH	338 mV @ 10 mA/cm ²	47	(Song & Hu, 2014)
NiFe-NS	1 M KOH	302 mV @ 10 mA/cm ²	40	(Song & Hu, 2014)
Fe _x Ni _y OOH-20F	1.0 M KOH	280 mV @ 100 mA/cm ²	66.7	(Xiao et al., 2021)
Ir/C	1.0 M KOH	370 mV @ 100 mA/cm ²	82.2	(Xiao et al., 2021)
NF (Ni Foam)	1.0 M KOH	382 mV @ 100 mA/cm ²	113	(Zhang et al., 2023)
NM (Ni Mesh)	1.0 M KOH	398 mV @ 100 mA/cm ²	125	(Zhang et al., 2023)
Ni(OH) ₂ @NF	1.0 M KOH	387 mV @ 100 mA/cm ²	97	(Zhang et al., 2023)
Ni(OH) ₂ @NM	1.0 M KOH	359 mV @ 100 mA/cm ²	89	(Zhang et al., 2023)
Pt-Ni(OH) ₂ @NM	1.0 M KOH	269 mV @ 100 mA/cm ²	51	(Zhang et al., 2023)

From Table 1 it can be observed that all those catalysts present relatively high overvoltage at a current density of 100 mA/cm², which is a typical current density at which OER overvoltage is measured in laboratories, and a reason why OER is considered a very sluggish reaction in both PEMWE and AEMWE.

Many things affect OER electrocatalyst performance, for example nanostructures can increase the ECSA: Song & Hu (2014) via exfoliation developed nanosheets of NiFe, NiCo and, CoCo, of which NiFe (a 2D catalyst) outperformed commercial IrO₂ catalyst. NiFe alloys have been highlighted for their potential to be used as OER catalysts, as well as PtNi alloys for HER (Du et al., 2022). Stainless Steel (SS) contains Ni and Fe and it can be used as anode in AWE after surface pre-treatment methods that generate a surface catalyst layer (SCL) active for OER (Todoroki & Wadayama, 2023). As Todoroki & Wadayama explain in their review, the OER performance strongly depends on the chemical composition and microstructure of the SCL; eventually the surfaces comprised by NiFe-hydroxide-based SCLs show superior performances to Ni-based anodes. Todoroki & Wadayama (2019) had previously synthesized Ni-Fe

hydroxide nanofibers on 316SS substrate through a simple electrolysis process that showed better performances than standard OER catalysts.

Heterostructures also have advantages over standard catalysts thanks to the synergistic effect that neighboring atoms of different origin have on OER performance. Wang et al (2023) tested a high performing catalyst that presented an heterojunction formed by Ni₂P/Ni₇S₆, suggesting that the good performance compared to Ni₂P, Ni₇S₆ and Ni alone is a result of the synergistic effect of the high crystalline heterogenous interface and the unique maple leaf-shaped nanosheet structure with rich defect sites for the OER reaction. Similarly, Xu et al (2016) developed a Ni₃C/C catalyst, where the effective OER species was formed by the heterostructure NiO_x/Ni₃C/C. For this catalyst, Xu et al explain that NiO despite having catalytic activity it acts as an insulator, impeding the transfer of charges; Ni₃C is metallic and prevents this issue, meanwhile hybridizing with carbon further improves the particle morphology and the charge transport during OER.

Table 2. Performance of several catalysts used in HER under alkaline media

Catalyst (HER)	Electrolyte	η (mV) at j mA/cm ²	TS (mV/dec)	Ref
NS-Ru@NiHO/Ni ₅ P ₄	1.0 M KOH	16 mV @ 10 mA/cm ²	35.2	(K. Wang et al., n.d.)
Ru-NC-700	0.1 M KOH	-47 mV @ 10 mA/cm ²	14	(Lu et al., 2019)
Pt-Ni(OH) ₂ @NM	1.0 M KOH	31 mV @ 10 mA/cm ²	42	(Zhang et al., 2023)
Pt/C	0.1 M KOH	-125 mV @ 10 mA/cm ²	39	(Lu et al., 2019)
NiO/Ni-CNT	1 M KOH	80 mV @ 10 mA/cm ²	82	(Gong et al., 2014)
NF	1.0 M KOH	180 mV @ 10 mA/cm ²	117	(Zhang et al., 2023)
NM	1.0 M KOH	210 mV @ 10 mA/cm ²	121	(Zhang et al., 2023)
Ni(OH) ₂ @NF	1.0 M KOH	153 mV @ 10 mA/cm ²	108	(Zhang et al., 2023)
Ni(OH) ₂ @NM	1.0 M KOH	135 mV @ 10 mA/cm ²	97	(Zhang et al., 2023)

Table 2 show the performance of several catalysts for HER under alkaline media. Compared to OER, it is evident that the overvoltage is less in comparison, and the Tafel slope is less pronounced too. Small amounts of PGM metals like Ru organized in single atoms and clusters of atoms can have big synergistic effects towards HER as demonstrates Wang et al (n.d.) and Pt doping in ultra-low quantities can present really good performances as describe Zhang et al (2023). NiO also presents catalytic activity towards HER as Gong et al (2014) demonstrated by developing an heterojunction-like structure of NiO/Ni over mildly oxidized carbon nanotubes which prevented the reduction of the nickel oxide, producing a PGM-free catalyst with activity close to commercial Pt/C catalyst.

Membranes and ionomers for AEMWE

PAP: Poly (aryl piperidinium)

PiperION is a commercial AEM based on poly (aryl piperidinium) commercialized by Versogen (formerly W7energy) (“Versogen - Our Revolutionary Membranes Offer Durability and Performance,” n.d.) and has been used in the AEM community with good results. Poly (aryl piperidinium) or PAP ionomers are formed by intercalating aryl chains containing biphenyl (BP) or terphenyl (TP) with a substituted form of piperidinium and trifluoroacetophenone monomer. By adjusting the proportion of piperidinium and trifluoroacetophenone, and by choosing between a BP or TP backbone, a big number of configurations of PAP polymer with changing characteristics can be produced (J. Wang et al., 2019). Wang et al found that PAP-TP-85 where 85 is the percentage of piperidinium substituted backbones provides the best hydroxide conductivity while having lower swelling compared to BP based backbone PAP polymers. The chemical structure of PAP-TP-85, the polymer used in PiperION is in Figure 5.

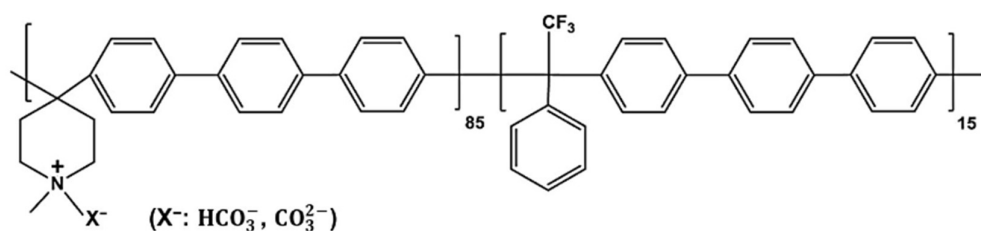


Figure 5. Chemical structure of PiperION TP-85 membrane (Endrődi et al., 2020)

Caielli et al (2023) in their experiment synthesized PBP membranes and showed that they could achieve very high conductivities, up to 185 ms/cm at 80 °C, superior to PiperION membranes, although not reaching the same superior mechanical properties. Still, the PBP membranes showed mechanical properties similar to other commercial AEM membranes and presented higher performance than commercial PiperION membranes.

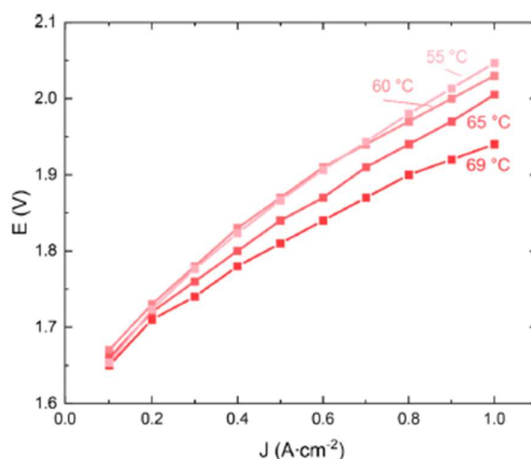


Figure 6. Influence of temperature on a pure water-fed electrolyser with PiperIon 50 μm MEA (Lindquist et al., 2021)

Lindquist et al (2021) compared the performance of PiperIon, Aemion and Sustainion membranes under identical conditions and found that PiperIon performed the best, highlighting the ability of PiperIon to work at high temperatures up to 90 °C, allowing for better performances compared to other membranes that degrade quickly at these high temperatures. Figure 6 shows the influence of temperature on electrolyser performance.

Xiao et al (2021) tested an oxygen evolution electrode with poly (aryl piperidinium) hydroxide exchange membrane and ionomers in a pure water fed electrolyser, reporting a performance of 1020 mA/cm² at 1.8 V, and proving continuous operation for 160 h at 200 mA/cm². A high performing cell was designed by Tricker et al (2023) who reported a PGM-free AEM cell using a 30 µm PiperionA AEM with a performance of 1.6 A/cm² at 2 V in 1 M KOH, and proved that it could last 515 h with negligible performance loss at 1.5 A/cm² in 0.1 M KOH. Chen et al (2021) obtained exceptional performances up to 7.68 A/cm² at 2 V and 1 M KOH by using a PAP variant. Chen et al explain that electrode design is crucial for reaching this high performance, as well as polymers with high water transport properties that allow for operation with optimal configurations. Table 3 summarizes the performance of AEMWE cells that use PAP polymers.

Table 3. Performance of AEMWE cells using PAP polymers

Anode	Cathode	Membrane and electrolyte	Performance and temperature	Reference
Co ₃ O ₄	NiCo	PiperionA 30 µm 1 M KOH	1.6 A/cm ² at 2 V (80 °C)	(Tricker et al., 2023)
Fe _x Ni _y OOH-20F	Pt/C	PAP-TP-85 20 µm Pure water	1020 mA/cm ² at 1.8 V (90 °C)	(Xiao et al., 2021)
Ni-Foam	Pt/C 0.5 mg/cm ²	PiperIon 80 µm 1 M KOH	0.3 A/cm ² at 1.8 V (60 °C) 0.62 A/cm ² at 2.0 V (60 °C)	(Caielli et al., 2023)
Ni-Foam	Pt/C 0.5 mg/cm ²	PiperIon 40 µm 1 M KOH	0.38 A/cm ² at 1.8 V (60 °C) 0.87 A/cm ² at 2.0 V (60 °C)	(Caielli et al., 2023)
Ni-Foam	Pt/C 0.5 mg/cm ²	PBP 60 µm 1 M KOH	0.18 A/cm ² at 1.8 V (60 °C) 0.58 A/cm ² at 2.0 V (60 °C)	(Caielli et al., 2023)
Ni-Foam	Pt/C 0.5 mg/cm ²	PBP 15 µm 1 M KOH	0.56 A/cm ² at 1.8 V (60 °C) 1.25 A/cm ² at 2.0 V (60 °C)	(Caielli et al., 2023)
IrO ₂	Pt/C	PiperIon TP-85 50 µm Pure water	1.00 A/cm ² at 2.0 V (65 °C)	(Lindquist et al., 2021)
Ni-Fe 20 mg/cm ²	Ni-Fe 20 mg/cm ²	PFTP-13 30 µm 1 M KOH	1.60 A/cm ² at 2.0 V (80 °C)	(Chen et al., 2021)
IrO ₂ 2 mg/cm ²	Pt/C 0.5 mg/cm ²	PFTP-13 30 µm Pure water	1.80 A/cm ² at 2.0 V (80 °C)	(Chen et al., 2021)
IrO ₂ 2 mg/cm ²	Pt/C 0.5 mg/cm ²	PFTP-13 30 µm 1 M KOH	7.68 A/cm ² at 2.0 V (80 °C)	(Chen et al., 2021)

PNB: Poly (norbornene)

PNB AEMs are usually identified by a first number that corresponds to the percentage of halogenated monomer used during the fabrication process and a second number that refers to the percentage of crosslinker used (N. Shah et al., 2023). Crosslinking decreases the polymers ion exchange capacity (IEC) but if done in small amounts the small decrease in conductivity is compensated by excellent mechanical stability and excellent performance at least in FC applications (Huang et al., 2019). The chemical structure of Pention AEM and of crosslinked PNB polymer is presented in Figure 7.

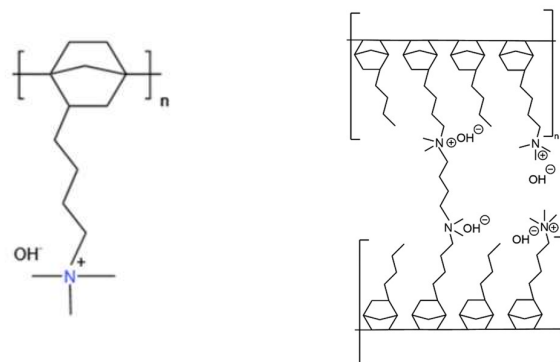


Figure 7. Chemical structures of Pention and of crosslinked PNB polymer (Z. Wang et al., 2023), (N. Shah et al., 2023)

Table 4 summarizes the performance of some AEMWE cells that make use of PNB based AEMs.

Table 4. Performance of AEMWE cells using PNB polymers

Anode	Cathode	Membrane and electrolyte	Performance and temperature	Reference
RP/SP Perovskite LaSr _{2.7} Co _{1.5} Fe _{1.5} O ₁₀	Pt/C	Pention-72-05 50 μm 6 M KOH	2.01 A/cm ² at 2.00 V (60 °C) 3.00 A/cm ² at 2.19 V (60 °C)	(Tang et al., 2022)
RP/SP Perovskite LaSr _{2.7} Co _{1.5} Fe _{1.5} O ₁₀	RP/SP Perovskite LaSr _{2.7} Co _{1.5} Fe _{1.5} O ₁₀	Pention-72-05 50 μm 6 M KOH	2.00 A/cm ² at 2.28 V (60 °C) 3.00 A/cm ² at 2.42 V (60 °C)	(Tang et al., 2022)
NiFe ₂ O ₄ 0.5 mg/cm ²	Pt ₃ Ni 1.2 mg/cm ²	GT75 40 μm 0.1 M NaOH	1 A/cm ² at 1.769 V (60 °C)	(N. Shah et al., 2023)
NiFe ₂ O ₄ /SS	NiFeCo/Ni fiber	V-1.5-O-1 40-50 μm 1 M KOH	0.868 A/cm ² at 2.0 V (60 °C)	(T. Wang et al., 2023)
NiFe ₂ O ₄ /SS	NiFeCo/Ni fiber	V-1.5-O-1 40-50 μm 0.1 M KOH	0.601 A/cm ² at 2.0 V (60 °C)	(T. Wang et al., 2023)

Wang et al (2023) studied the effects of water activity and temperature in three high performance AEMs like Alkymer, Orion and Pention: In general, the water uptake and

equilibrium water content of these AEMs is not strongly affected by temperature and mostly just by water activity; additionally, the conductivity of these AEMs was found to depend both in equilibrium water content λ and also on temperature. The Pention membrane studied by Wang et al had an IEC of 3.50 and it was 30 μm thick. The equilibrium water content λ of Pention as a function of water activity can be found in Equation 3, and the Arrhenius-type relationship for the ionic conductivity of Pention in Equation 4.

$$\lambda_{\text{Pention}} = 20a^3 - 18.86a^2 + 8.38a, \quad 0 < a \leq 1$$

Equation 3. Pention equilibrium water content (Z. Wang et al., 2023)

$$\sigma_{\text{Pention}} = \begin{cases} (0.32\lambda^2 - 1.88\lambda + 3.35) \\ \exp \left[1450.23 \left(\frac{1}{343.15} - \frac{1}{T} \right) \right], \\ 3.48 \leq \lambda \leq 9.52 \\ 0.20\lambda \exp \left[1450.23 \left(\frac{1}{343.15} - \frac{1}{T} \right) \right], \\ 0 \leq \lambda < 3.48 \end{cases}, \quad 333.15 \leq T \leq 353.15$$

Equation 4. Pention ionic conductivity (Z. Wang et al., 2023)

Other AEM membranes

Kang et al (2022) reported Orion AEM having the best performance among all commercial AEMs that they tested, including Fundtech's FAA-3 membrane. A summary of results with different AEMs to the ones that have been reviewed so far is presented in Table 5.

Table 5. Performance of AEMWE cells using other membranes

Anode	Cathode	Membrane and electrolyte	Performance and temperature	Reference
IrO_2 2 mg/cm ²	Pt/C 0.4 mg/cm ²	Orion TM1 30 μm 1 M KOH	2.75 A/cm ² at 1.9 V (70 °C)	(Kang et al., 2022)
IrO_2 2 mg/cm ²	NS-Ru	FAA-3-PK-130 1 M KOH	1.0 A/cm ² at 1.7 V (50 °C)	(K. Wang et al., n.d.)
$\text{Ni}_2\text{P}/\text{Ni}_7\text{S}_6$	Pt/C 4 mg/cm ²	FAA-3-50 1 M KOH	1 A/cm ² at 1.88 V (75 °C)	(F.-L. Wang et al., 2023)
NiFe_2O_4	Pt/C	FAA-3-50 1 M KOH	1.43 A/cm ² at 1.8 V (60 °C) 2.35 A/cm ² at 2 V (60 °C)	(Martinez-Lazaro et al., 2023)
Stainless Steel	Pt/C 0.5 mg/cm ²	Sustainion X37-50 1 M KOH	2.74 A/cm ² at 2.0 V (70 °C)	(Faqeeh & Symes, 2023)

Hydration in AEMs is characterized by the water content λ which corresponds to the number of water molecules per positive charged group in the polymer; Schroeder's paradox corresponds to the concept that water content is much higher when the membrane is in contact with liquid water compared to gas with 100% relative humidity and it is very pronounced in AEM polymers (Luo et al., 2020). As Luo et al explain, hydration is an important variable that affects ion conductivity of the membranes and in their article, they report that PAA membranes present superior ion conductivity that Fumasep's FAA3 membranes.

Conductivity also depends on the counter-anion that is being transported. In both PAP and FAA3 membranes, ion conductivity is much higher for hydroxide than for carbonate or bicarbonate anions (Luo et al., 2020). This effect is critical in AEM fuel cells because they run with ambient air that contains CO₂, which ultimately replaces the more mobile hydroxide anions with sloppier carbonate and bicarbonate forms (Ziv et al., 2019).

Interaction of materials and system configuration

Electrode design is critical for developing high performance AEMWE cells. The content and type of ionomer can have a huge influence in cell performance as Chen et al (2021) describe in their work. In one of their experiments, they varied the ionomer content in the cathode from 10% to 40% finding that the optimal value in their case was 25%. By using a system configured with an anhydrous cathode and several design optimizations including the optimized ionomer content in cathode is how they were able to reach the exceptional performance of 7.68 A/cm² at 2 V. For anhydrous cathode operation it is important to use polymers that can allow the necessary water transport to provide the cathode with water as Chen et al explain. Tricker et al (2023) reached a similar conclusion, and demonstrated how anhydrous cathode, the one where water and electrolyte is only supplied through the anode, is the best performing configuration for their AEMWE system.

Tricker et al (2023) in their work investigate three critical properties including catalyst loading, microporous-layer (MPL) loading, and GDL hydrophobicity. Their experiments show that there is an optimal catalyst loading that balances kinetic and mass transport; and that adding an MPL to the GDL improves the kinetic performance of the cathode but shows only marginal influence at high current densities, and further increasing results in small loss in performance. The other property studied by Tricker et al is the impact of GDL hydrophobicity: They varied the polytetrafluoroethylene (PTFE) content in the GDL and found that increasing it helps to prevent liquid-water accumulation and improves gas transport through the GDL. They observe that a large improvement is seen when hydrophilic GDL is switched to hydrophobic concluding that H₂ bubble removal rather than water supply on cathode impacts cell performance more, especially at high current densities.

Another use of ionomer is to bind in place the catalyst particles in the electrode and to prevent detachment. Osmieri et al (2023) observed LSC (La-Sr-Co oxide) catalyst detachment when exposed to deionized (DI) water while preparing a catalyst covered substrate electrode (CCS). To avoid the detachment, the catalyst ink composition was modified by adding Nafion ionomer,

which is known to have good binding properties; interestingly they didn't observe detachment caused by using DI water in PGM catalysts, speculating that the AEI interacts differently with different catalysts. Osimieri et al also explain that careful tuning of the anode catalyst ink formulation is necessary for assuring good performance of MEAs with the LSC catalyst at the anode: CL with lower binder-to-ionomer ratio had a considerable improvement of performance likely because the acidic Nafion binder neutralizes the functional groups present in the AEI that are responsible for OH⁻ transport.

Catalyst layers can be present in two different configurations in the MEA: As catalyst-coated membranes (CCM) and as catalyst-coated substrate (CCS). Ito et al (2018) in their electrolysis experiment found that the most appropriate electrode configuration in their case is CCM-cathode and CCS-anode, adding that there is also an optimal catalyst loading and binder content in the CL.

Fundamentally, the importance of finding a good balance in materials lies in the triple phase boundary area in the electrode, the area where electron, ionic and gas transport takes place. Liquid electrolytes like KOH increases the triple phase boundary area in the electrode for electrochemical reactions, and increasing the concentration up to 6 M resulted in progressive improvement in performance for perovskite-based electrocatalysts prepared by Tang et al (2022). Santoro et al (2022) explain that data seems to show that both PGM and PGM-free anode electrocatalysts are not in direct contact with the AEI (associated with high local pH) during operation of AEMWEs but are instead indirectly connected to the AEI network via the liquid. Figure 8 provides an illustration of this process.

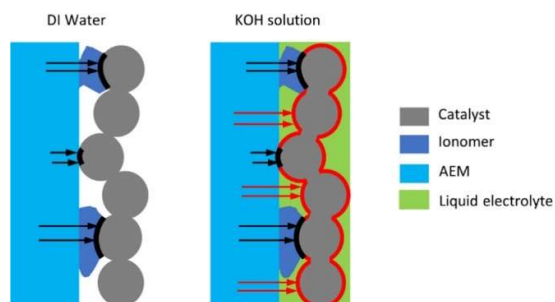


Figure 8. Illustration of ion-transport pathways of a half cell (anode) when DI water and KOH solutions are fed to the AEM electrolyzers (Liu et al., 2021)

Liu et al (2021) provide great insight about the role of electrolyte in AEMWE: In their experiment, the total effective electrochemical active surface area (ECSA) in the cell with 1 M KOH was five times higher than that of the cell with DI water, and more than 80% of the reaction current was associated with the liquid electrolyte. They also found that increasing the KOH concentration significantly increases OER kinetics through additional ion-transport pathways, and increased ECSA and OER activity, but it marginally increases HER kinetics. They conclude that the effect of electrolyte on OER kinetics might be more important than the effect on AEM conductivity, and that optimal CL formulations and high ECSA is critical for the development of AEMWEs operating without electrolyte.

Importantly, AEM, anode AEI and cathode AEI not necessarily have to share the same properties and they can be tuned differently according to the function that they perform inside

the electrolysis cell. Liu and Weber (2022) examined the role of HEI and HEM for HEMWEs and concluded that increasing the water diffusion coefficient and reducing the electroosmotic coefficient of the HEM is beneficial for the performance as it helps to supply reactant water to the cathode and hydrate HEM and cathode catalyst layer HEI; in contrast, lower water diffusivity of the cathode catalyst layer HEI helps to retain more reactant water in the high reaction rate region next to the HEM, thus increasing performance. This effect is illustrated in Figure 9. They also suggest that distributing more ECSA next to the HEM or making denser but thinner anode catalyst layers improves the performance by reducing the anode ohmic and kinetic losses.

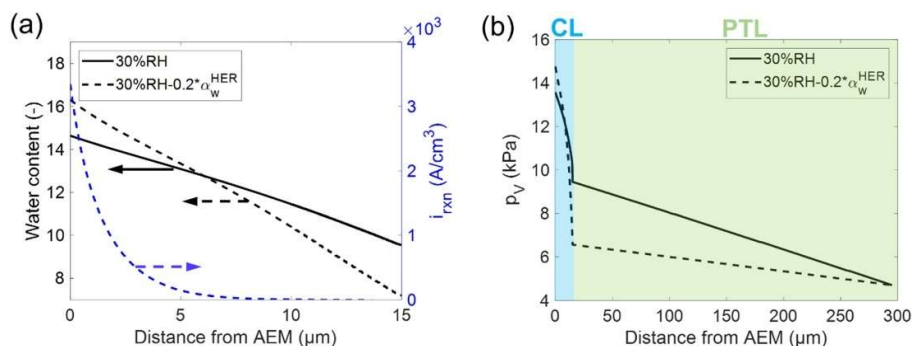


Figure 9. (a) Water content and reaction current density distribution in the cCL. (b) Water vapor partial pressure in the cCL and cPTL at $0.5 A/cm^2$ for cells with different cCL HEI properties (Liu & Weber, 2022)

The observations of Liu and Weber (2022) are really interesting because it permits to understand better how operating with an anhydrous cathode can be advantageous provided that the thin CL region next to the AEM is maintained well hydrated. In their experiment working with a dry cathode Tricker et al (2023) conclude that water back-diffusion from the anode to the cathode can be a preferred pathway to supply water to the cathode compared to direct electrolyte feed even at high current densities. Not only that, but Tricker et al in an experiment using DI water also found that by lowering the RH of the H_2 feed at around 80% maximum performance was obtained, concluding that a higher water gradient between anode and cathode facilitates water back-transport.

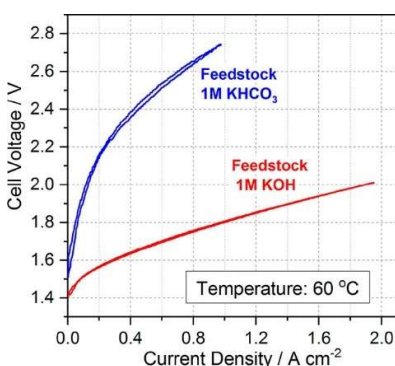


Figure 10. AEMWE cell performance comparison at $60\text{ }^\circ\text{C}$ using $1\text{ M }KHCO_3$ and $1\text{ M }KOH$ as feedstock (L. Wang et al., 2019)

Figure 10 illustrates the effect of electrolyte selection: after replacing the feedstock from $1\text{ M }KOH$ to $1\text{ M }KHCO_3$ the cell voltage sharply increases for the same current density. For Wang et al (2019) the reasons for this change are the decreased ion conductivity in the AEM due to

buildup of carbonates and the lower catalytic activity of Ni-based catalysts in lower pH environments: 1 M KHCO_3 has a pH value of about 8, compared to the value of 14 for 1 M KOH electrolyte. It is important to note that in Wang et al experiment, they elaborated plasma-sprayed electrodes without any binders or precious metals, and hence all the interface between the electrodes and AEM was provided only by the electrolyte.

Carbonates have lower ionic mobility than hydroxide ions, though they have the positive effect of increasing AEM chemical stability since carbonate anions are weaker nucleophiles than hydroxide anions (Ziv et al., 2019). Using potassium carbonate as electrolyte in AEMWEs can increase the durability of the device thanks to the less corrosive environment compared to potassium hydroxide but at the cost of performance, and because of carbonation issues, a more conductive AEM and ionomer may be essential for these types of systems as well as more active catalysts under the lower pH condition (Li et al., 2021). Regarding pure water operation, one obstacle stems from the fact that the performance of the most extensively studied Ni catalysts degrades considerably below pH 9 (Vinodh et al., 2023). Pourbaix diagrams in Figure 11 can illustrate the effect of pH in the stability of metals used in OER catalysts. As Du et al (2022) explain, these diagrams can provide insights and initial material stability guidelines for catalysts, while not forgetting that the stability of a catalyst is also influenced by its chemical and physical structure, including physical size.

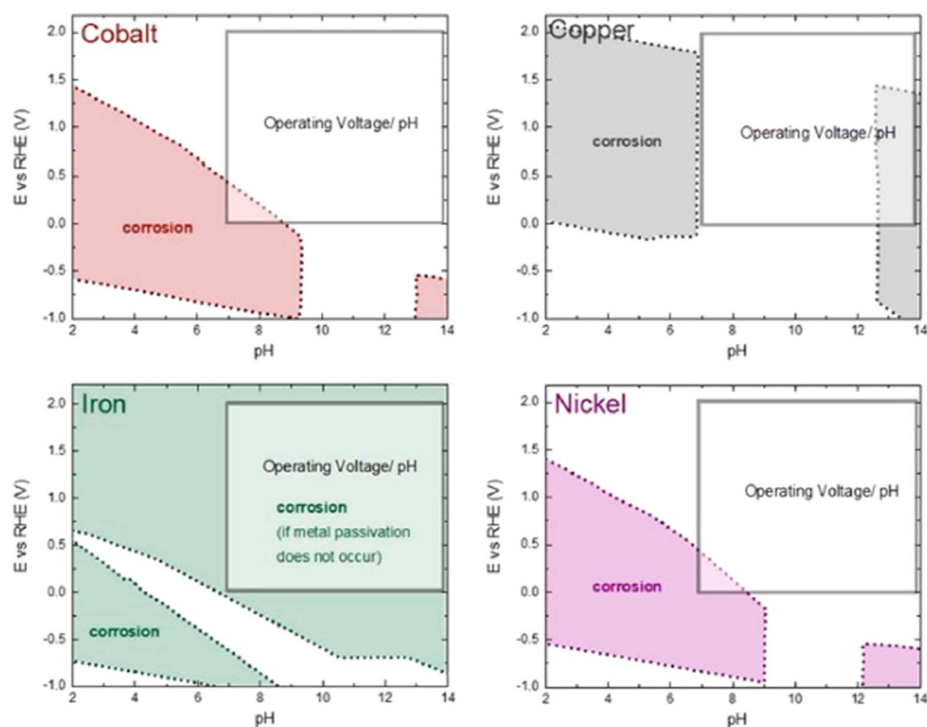


Figure 11. Pourbaix diagrams of cobalt, copper, iron, and nickel in aqueous electrolytes at ambient pressure and 25 °C (Du et al., 2022)

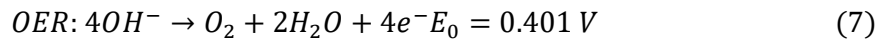
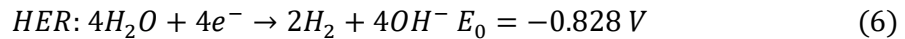
Methodology

Anion Exchange Membrane Water Electrolysis Cell

Figure 12 illustrates an AEMWE cell. The cell works by applying a voltage greater than the Nerst potential of the reaction for water electrolysis between two electrodes (5).



By providing water and hydroxide anions to the electrodes, the HER and OER reactions take place in the cathode and anode respectively (6),(7):



From (6) we can observe that water is consumed and hydroxide anions are produced at the cathode; from (7) hydroxide anions are consumed and water is produced at the anode. Electrons are transferred from anode to cathode through the metallic phase of the electrodes and through the voltage source. The electrical circuit is completed by the flow of negative hydroxide ions from cathode to anode through an electrolyte. In AWE the electrolyte is usually a high concentration solution of KOH. In AEMWE, an anion exchange membrane is used instead, although a supporting KOH solution is still frequently used.

The produced gases are then ejected in combination with the water/electrolyte flow that it is fed into each electrode. The gases don't intermix thanks to the membrane that acts as separator. HER and OER reactions occur on the surface of active catalysts in a region called the triple-phase boundary (TPB) where electrons, gases and ions interact in their vicinity with each other.

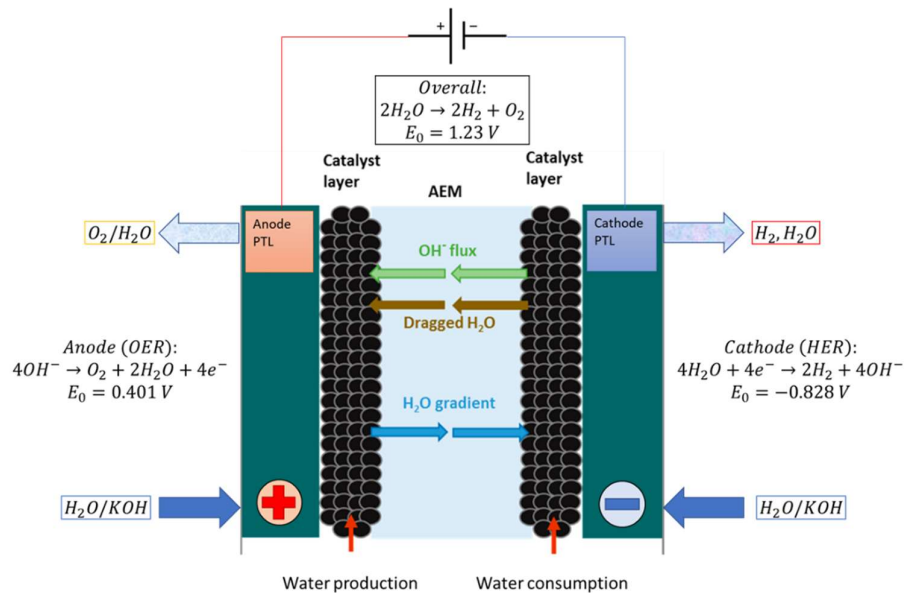


Figure 12. Diagram of an AEMWE Cell, adapted from (Zheng et al., 2018)

Experimental setup

Figure 13a is a diagram of the experimental setup used. It consists of a AEMWE cell of 25 cm² of area; an electrolyte feeding circuit with a pump and electrolyte reservoir; a reference electrode wedged into the cell; a power supply; one multimeter for measuring cell voltage and one multimeter for measuring the reference voltage; a thermal bath to maintain constant temperature; and a high frequency resistance (HFR) meter. The final setup can be observed in Figure 13b.

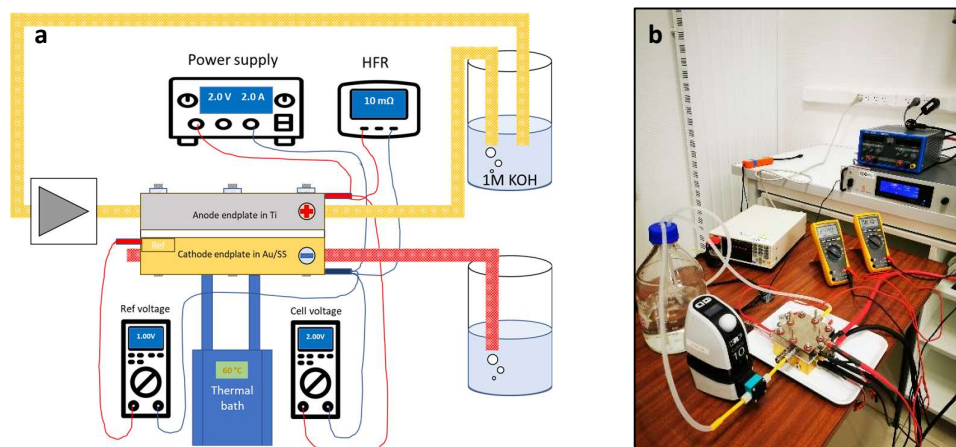


Figure 13. Experimental setup

Figure 14 shows the two types of membranes used in the experiments. PiperIon A80 80 μm (Versogen) in bicarbonate form was used for the first test. For the second test, a Pention-75-15CL AEM CCM of 30 μm thickness fabricated by XERGY was used. The catalyst content of the latter CCM is 3 mg IrRuO_x and 3 mg PtB for anode and cathode respectively.



Figure 14. Piperlon (a) and Pention (b) AEMs

Figure 15 shows the components of the cell. The PTLs used are 1mm thick 25cm² Ni-Alloy asymmetric electrodes for alkaline water electrolysis from Light Bridge (Light Bridge, n.d.). MEAs are sandwiched between a gold coated stainless steel (cathode) and titanium (anode) endplates with external temperature control fabricated in LEMTA. The cathodic endplate possesses an isolated inset with a hydrogen channel that forms the metallic phase for the reference electrode. The thickness of the MEA after compression is 80% of the initial thickness, achieved by using hard substrate gaskets totaling 1.6 mm thickness. The cell was tightened with 5 Nm of torque on each bolt.

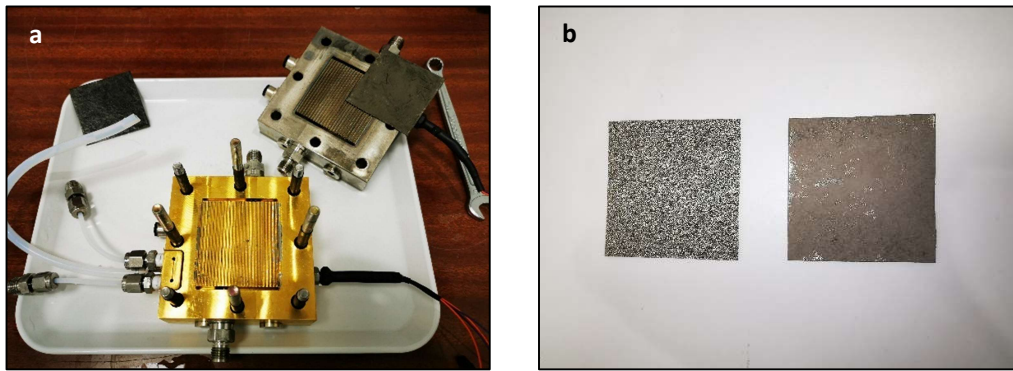


Figure 15. Endplates (a) and PTLs (b) showing both sides

Three configurations were tested: Figure 16a and Figure 16b illustrate two cells with gas diffusion electrodes (GDE) where the chemical reaction is catalyzed by the Ni-alloy PTLs themselves. The MEA is completed with a PiperIon A80 AEM with 80 μm thickness. For cell #1 (Figure 16a) the electrolyte is supplied through the anode while for the cell #2 (Figure 16b) the electrolyte is supplied through the cathode. The cell #3 (Figure 16c) uses a CCM with IrRuO_x catalyst on the anode and PtB catalyst on the cathode. The membrane used in this cell is Pention-75-15CL with 30 μm thickness and the electrolyte is supplied through the anode just like cell #1. Hydrogen gas produced by cells #1 and #3 is passed through the reference electrode to provide the necessary redox species to form a reversible hydrogen electrode (RHE). No reference electrode measurements were taken for cell #2.

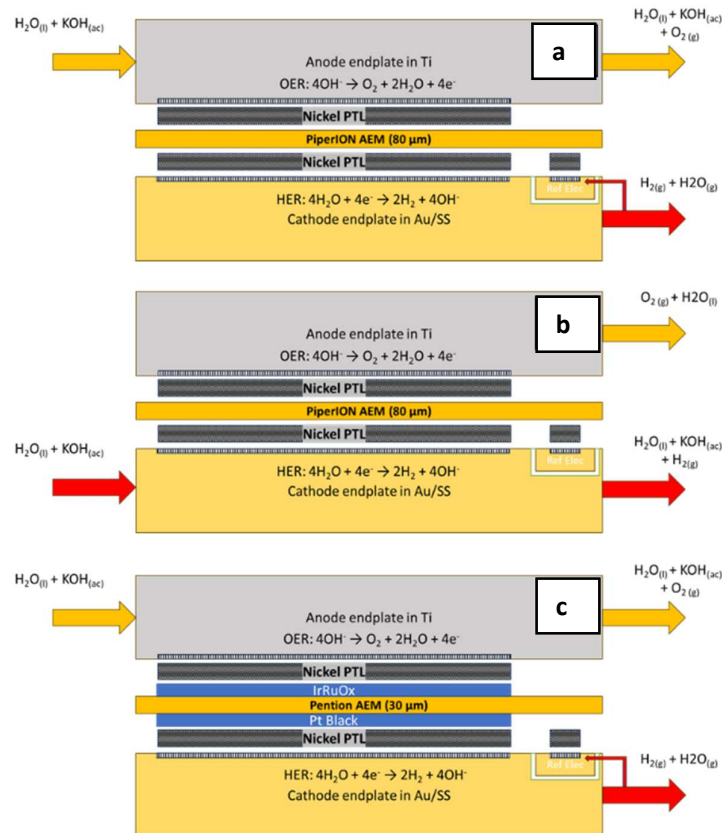


Figure 16. Cell configurations used during the experiments

AEMWE characterization

For cells #1 and #2, 1 M KOH solution was pumped overnight to hydrate and convert the membrane to hydroxide form. Polarization curves were taken by increasing the voltage by approximately 0.1 V steps until a maximum value, and waiting 1 minute before taking the reading. Voltage was then decreased by the same voltage step, but waiting only 30 seconds between each reading as the current stabilized faster compared to when voltage was increased. Polarization curves were taken at different temperatures. Constant temperature during measurements was achieved by using a thermal bath. HFR measurements were taken at 1 KHz frequency when no voltage was applied, at the beginning and end of each polarization curve.

For cell #3, 1 M KOH solution was pumped through the cell two hours before taking the polarization curves. For the polarization curves, voltage steps of 0.05 V were used and current was allowed to stabilize for approximately 1 minute before reading each value.

Electrode potentials

In the context of this work, the potential of an electrode is defined as the difference between the potential of the metallic phase ϕ^m and that of the electrolyte ϕ^e surrounding it (Parra-Restrepo, 2020). The potentials for the anode and the cathode are given by (8) and (9).

$$E_a = \phi_a^m - \phi_a^e \quad (8)$$

$$E_c = \phi_c^m - \phi_c^e \quad (9)$$

In the absence of current, the potential of the cell U_{cell} is equal to the difference between the potential of the anode and of the cathode (10); the potential across the electrolyte is homogeneous and thus it has the same value at the vicinity of both electrodes (Parra-Restrepo, 2020):

$$U_{cell} = E_a - E_c = \phi_a^m - \phi_c^m \quad (10)$$

Parra-Restrepo (Parra-Restrepo, 2020) in his thesis explain that for PEM electrolysis, in the presence of current, protons pass from the anode towards the cathode thanks to a negative gradient of potential in direction to the cathode ($\phi_a^e > \phi_c^e$), and that the resistance of the electrolyte to the circulation of protons is expressed with Ohm's law. This remains true for AEM electrolysis, however in this case it is negative ions that circulate from cathode to anode instead. This process is illustrated in Figure 17, and is expressed in equation (11).

$$U_{cell} = E_a - E_c + IR = \phi_a^m - \phi_a^e + IR - (\phi_c^m - \phi_c^e) \quad (11)$$

In equation (11) R represents the resistance of the membrane and the resistance to the crossing of electrons from other components, and I represents the current. Usually the resistance of the components can be ignored and only that of the membrane is taken into account (Parra-Restrepo, 2020).

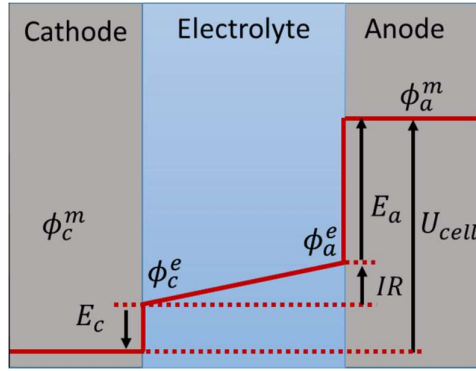


Figure 17. Representation of electrode potentials in PEM water electrolysis in presence of current (Parra-Restrepo, 2020)

In Figure 13a it can be appreciated that one key measurement during experiments is the difference of potential between the reference electrode and the cathodic endplate. This difference of potential can be called the measured cathode potential or E_c^{mes} (12).

$$E_c^{mes} = \phi_{ref}^m - \phi_c^m \quad (12)$$

The hydrogen electrode is the best candidate for reference electrodes in aqueous solutions, the involved hydrogen reaction takes the form (13), and the potential of the electrode as a function of pH at 1 bar of pressure is given by equation (14) (Cazot, 2019). The potential of the reference electrode is defined in equation (15).



$$E_{ref} = E_{H^+/H_2} = E^0 - 0.06 \text{ pH} \quad (14)$$

$$E_{ref} = \phi_{ref}^m - \phi_{ref}^e \quad (15)$$

The Standard Hydrogen Electrode (SHE) is defined with the condition of an ideal solution at pH 0, and for this electrode the value E^0 is conventionally taken as 0 V; the Reversible Hydrogen Electrode (RHE) is obtained by supplying hydrogen gas on a platinum surface so that the equilibrium defined in (13) can occur (Cazot, 2019).

With equation (15) we can rewrite equation (12) in terms of the electrolyte that is in contact with the metallic phase of the reference electrode (16).

$$E_c^{mes} = E_{ref} + \phi_{ref}^e - \phi_c^m \quad (16)$$

Based on Figure 17 if we place the reference electrode in the membrane, it can be in contact with electrolyte at any potential between ϕ_a^e and ϕ_c^e . If the cell electrodes are perfectly aligned and the reference electrode is placed far away from the influence of the anode and the cathode, ϕ_{ref}^e will be positioned exactly at half the total difference of potential across the membrane ($\phi_a^e - \phi_c^e$). This is represented in Figure 18. This is however not always the case. If the electrodes are not well aligned the reference electrode can measure any other potential in between (Cazot, 2019). By introducing an ohmic compensation factor CF (17) that defines how much of the total IR drop across the membrane corresponds to the IR drop between the reference electrode and the anode, we can formulate equations (18) and (19). In the case of perfect electrode alignment CF should equal 0.5.

$$CF = \frac{(\phi_a^e - \phi_{ref}^e)}{(\phi_a^e - \phi_c^e)} \quad (17)$$

$$(\phi_a^e - \phi_{ref}^e) = IR \times CF \quad (18)$$

$$(\phi_{ref}^e - \phi_c^e) = IR \times (1 - CF) \quad (19)$$

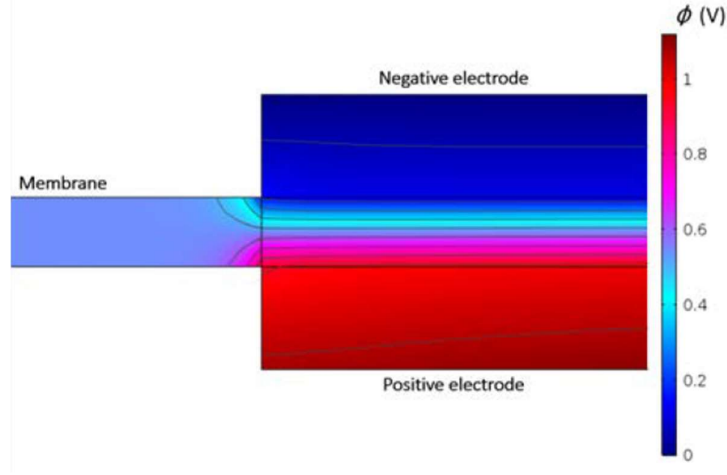


Figure 18. Numerically resolved potential distribution in the three phases and isopotential lines for the case of perfect alignment of the two electrodes (Cazot, 2019)

By combining equations (9), (16) and (19) we can finally obtain the potential of the cathode E_c as a function of measurable variables (20). The potential of the anode E_a (21) can be obtained from (11). The overvoltage for each electrode can be obtained by subtracting the corresponding redox couple potential and is explained in the next section.

$$E_c = E_{ref} - E_c^{mes} + IR \times (1 - CF) \quad (20)$$

$$E_a = U_{cell} + E_c - IR \quad (21)$$

Procedure for calculating the electrode potentials from reference electrode data

To obtain the electrode potentials we need R , CF and E_{ref} for equation (20). The cell resistance R can be obtained from either measuring the HFR or by fitting the polarization curve at high current densities, where the voltage has a linear relationship with current density as expressed in Ohm's law (22). The Area Specific Resistance (ASR) is obtained in MATLAB by applying the fit function to the linear segment of the polarization curve (Figure 19a).

$$\eta_{ohmic} = i \times ASR \quad (22)$$

With ASR information, the next step is to find appropriate values for CF and E_{ref} . This process is illustrated in Figure 20. First, we start by assuming CF equal to 0.5 and E_{ref} equal to 0 V. This is analogous to say that the electrodes are perfectly placed and that the reference electrode

electrolyte is an ideal solution of pH 0. Then the potentials of the cathode and anode can be calculated from (20) and (21) and the result is illustrated in Figure 19b.

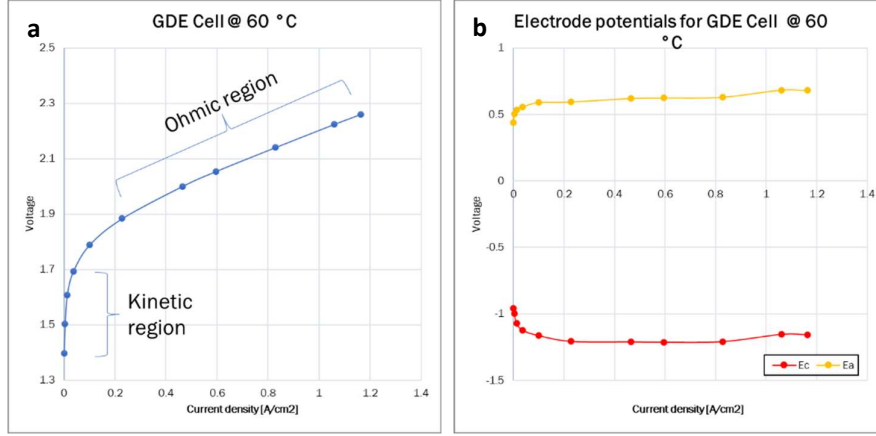


Figure 19. (a) Illustration of ohmic region and kinetic region for an AEMWE cell (b) example of deduced electrode potentials for the same cell

The overvoltage for the cathode (23) and anode (24) is calculated individually from the electrode potentials obtained from (20) and (21).

$$\eta_c = E_c - E_{HER}(T) \quad (23)$$

$$\eta_a = E_a - E_{OER}(T) \quad (24)$$

Here E_{HER} and E_{OER} correspond to the potentials of the water reduction and hydroxide oxidation reaction respectively. These redox potentials are a function of temperature, pH and pressure of the chemical species. If we assume a pH of 14, and a working pressure of 1 for Hydrogen and Oxygen, then the potentials can be written as solely a function of temperature (in Celsius) (Tricker et al., 2023):

$$E_{HER} = -0.828 - 0.000836(T - 25) \quad (25)$$

$$E_{OER} = 0.401 - 0.0016816(T - 25) \quad (26)$$

Two criteria are applied in order to verify if any pair of values for CF and E_{ref} are reasonable:

1. The overvoltage for any electrode at zero current is equal to zero.
2. The overvoltage for any electrode is a monotonous non-decreasing function with current density.

The Butler-Volmer equation (27) can help verify the previous criteria. Two Butler-Volmer models are fit to the overvoltage calculated from (23) and (24) in the low current density region. The electron transfer coefficient α is taken as 0.5 and the MATLAB function *lsqcurvefit* is used to obtain the change current density i_0 for each electrode.

$$\eta = \frac{RT}{2\alpha F} \operatorname{asinh} \frac{i}{2i_0} \quad (27)$$

The errors (28) and (29) are calculated from comparing the overvoltage obtained from the two models to the overvoltage calculated from (23) and (24) across the full range of current as in Figure 20.

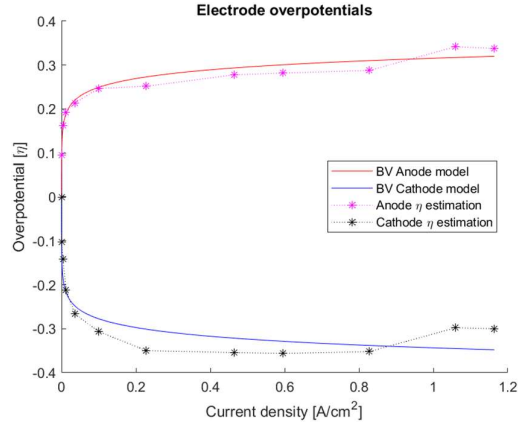


Figure 20. Corrected electrode potentials versus the Butler-Volmer model for each electrode. Example is for a cell operating at 60 °C

$$error_{anode} = \eta_a - \eta_{BV\ anode} \quad (28)$$

$$error_{catho} = \eta_c - \eta_{BV\ catho} \quad (29)$$

Additionally, a simple electrochemical model (30) considering only activation overvoltage (Butler-Volmer model) and ohmic overvoltage (Ohm's law) was built with the parameters obtained previously. The error between (30) and the performance data is calculated with (31).

$$U_{cell\ model} = E_{rev} + IR + \eta_{BV\ anode} + \eta_{BV\ cathode} \quad (30)$$

$$error_{model} = U_{cell} - U_{cell\ model} \quad (31)$$

The sum of the squared errors is calculated in (32). A script was written in MATLAB to iterate different values of CF and E_{ref} . The couple of values that minimized (32) were saved for each set of experimental data. This process is illustrated in Figure 21.

$$sse = \sum error^2 \quad (32)$$

temp	r_ohmic	i0_anode	i0_cathode	anode_ri	dpp_ref_SHE	sse_el_model	sse_electrodes	sse_total
61	0.363186356	5.17837E-07	6.158971029	0	0	0.436857837	0.633458445	1.070316
61	0.363186356	5.17837E-07	6.158971029	0	0	0.436857837	0.633458445	1.070316
61	0.363186356	7.08871E-07	0.030016208	0	-0.05	0.252109607	0.412734195	0.664844
61	0.363186356	2.77602E-06	0.005731603	0	-0.1	0.24534205	0.326825954	0.572168
61	0.363186356	7.82995E-08	0.001197292	0	-0.15	0.04556737	0.078805001	0.124372
61	0.363186356	1.48764E-06	0.000218209	0	-0.2	0.055014532	0.061123765	0.116138
61	0.363186356	2.46233E-06	3.84859E-05	0	-0.25	0.045343073	0.039623937	0.084967
61	0.363186356	1.61892E-05	6.71314E-06	0	-0.3	0.045176159	0.034549666	0.079726
61	0.363186356	9.19306E-05	1.18243E-06	0	-0.35	0.045177237	0.039985792	0.085163
61	0.363186356	0.000525025	5.40409E-07	0	-0.4	0.052738853	0.064327592	0.117066
61	0.363186356	0.003299295	1.70051E-07	0	-0.45	0.067069041	0.10237632	0.169445
61	0.363186356	0.026206086	1.37082E-06	0	-0.5	0.299196495	0.363677038	0.662874
61	0.363186356	6.05520239	3.25872E-07	0	-0.55	0.387903234	0.463525804	0.851429
61	0.363186356	13.10731138	1.54214E-07	0	-0.6	0.318643827	0.636230863	0.954875
61	0.363186356	16.27043276	2.09511E-06	0	-0.65	0.609379353	1.407650799	2.01703
61	0.363186356	22.63535387	3.51079E-07	0	-0.7	0.398862388	1.588009521	1.986872
61	0.363186356	29.00027477	2.45317E-07	0	-0.75	0.363129556	2.10516775	2.468297
61	0.363186356	35.36519583	7.40888E-07	0	-0.8	0.481172247	3.066109551	3.547282
61	0.363186356	28.13660934	1.75734E-07	0	-0.85	0.331513794	3.511805873	3.84332
61	0.363186356	32.42318883	6.89448E-08	0	-0.9	0.252860907	4.152915759	4.405777
61	0.363186356	36.70976833	5.98798E-07	0	-0.95	0.456919539	5.824842291	6.281762
61	0.363186356	40.99634782	5.99062E-07	0	-1	0.457053567	6.987264762	7.439318
61	0.363186356	1.61892E-05	6.71314E-06	0	-0.3	0.045176159	0.034549666	0.079726
61	0.363186356	1.65817E-05	6.60937E-06	0.05	-0.3	0.045176064	0.034887267	0.080063
61	0.363186356	1.69841E-05	6.44433E-06	0.1	-0.3	0.045176004	0.039776999	0.084953
61	0.363186356	1.73956E-05	6.24836E-06	0.15	-0.3	0.045176154	0.049153767	0.09433

Figure 21. Example of results from minimizing the sse for a data set obtained at 61 °C

Results, analysis and discussion

Performance of the cells

Figure 22 shows the influence of temperature in the performance of the cell #1 (refer to *AEMWE characterization* section of this report in page 21). At low temperature, small increments of temperature can have big impacts on performance as can be seen from the big jump in performance when changing from 30 °C to 40 °C. Increasing further the temperature increases the performance but with diminishing returns. From studying the plots, it can be deduced that the cell's ASR decreases with temperature as the slope of the polarization curve at high current densities decreases with increased temperature. It is worth mentioning that cell #1 is a PGM-free cell using a robust set of Ni-Alloy GDEs and a PiperIon AEM. Despite presenting low performance and relying on KOH electrolyte, it is easy to fabricate and it is a first step into developing better performing cells.

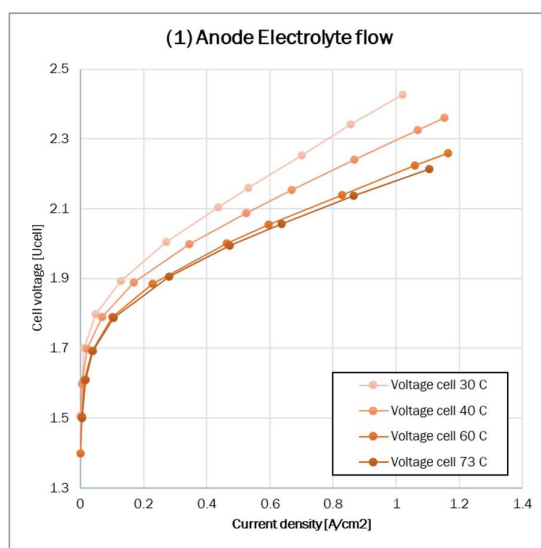


Figure 22. Polarization curves of the cell # 1 at different temperatures

Figure 23 compares the performance between cell #1 (fed through the anode) and cell #2 (fed through the cathode) at 60 °C. Cell # 1 requires lower voltages and has better performance than cell # 2 demonstrating that for this particular configuration feeding water and electrolyte only through the anode is advantageous, which is in line with what Chen et al (2021) and Tricker et al (2023) reported. Explanation for this can be found in the section *Interaction of materials and system configuration* in page 14. In that section it is explained that OER is especially susceptible to the presence of electrolyte (Liu et al., 2021), even more than HER, and that HER can benefit from high water transport across the membrane and low electroosmotic drag (Liu & Weber, 2022). All those conditions can be met when electrolyte is fed through the anode, but not when the cathode is used instead which can explain the higher overvoltages observed in cell #2. Feeding electrolyte through both electrodes would provide additional water and electrolyte to the cathode and this should reduce overvoltage at least at low current density when hydrogen

bubbles are still in low quantity. Using this last configuration was not tried and it could be done in future experiments to verify this hypothesis.

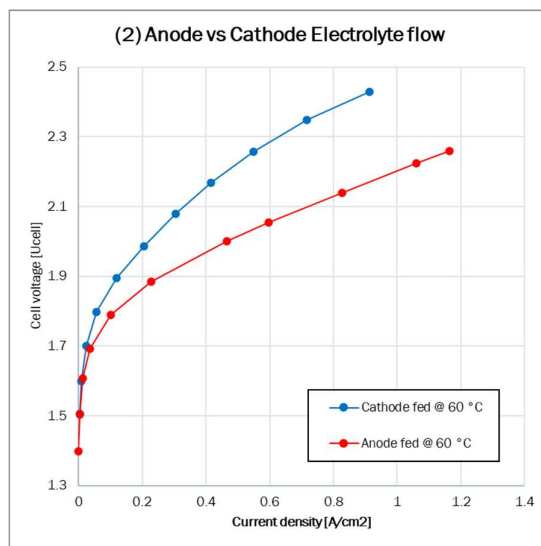


Figure 23. Performance comparison between cell # 1 (anode fed) and cell # 2 (cathode fed)

Figure 24 compares the performance between cell #1 (GDE, Ni-alloy catalyst) and cell #3 (CCM, IrRuO_x anode, PtB cathode) at 60 °C. Comparing the slopes at high current density it is evident that the ASR of cell # 3 is lower than that of cell # 1, which could be attributed at least partially to the difference in membrane thickness (30 μm vs 80 μm). Cell #3 showed a very respectable performance reaching a current density of 2.9 A/cm² at 2 V. In the next section, *Performance of the components* in page 29, it is shown that this high performance is partially thanks to the higher activity of PtB as HER catalyst.

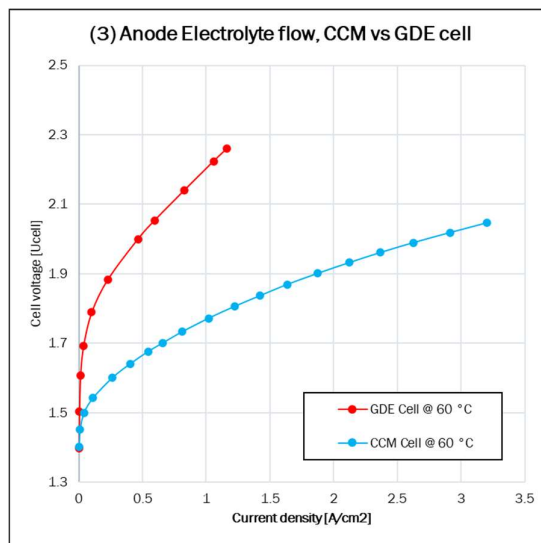


Figure 24. Performance comparison between cell #1 (GDE) and cell # 3 (CCM)

Figure 25 compares the efficiency between cell #1 and cell #3. Efficiency in this context is defined as the ratio between the energy content of hydrogen produced (calculated thanks to Faraday law) to the electrical energy used in the cell. It can be observed that efficiency always

decreases, and that cell #3 has higher efficiency than cell # 1. The disadvantage of configurations such as cell # 3 is that PGM materials like iridium are rare and expensive, hence, why non-PGM alternatives are gaining more interest.

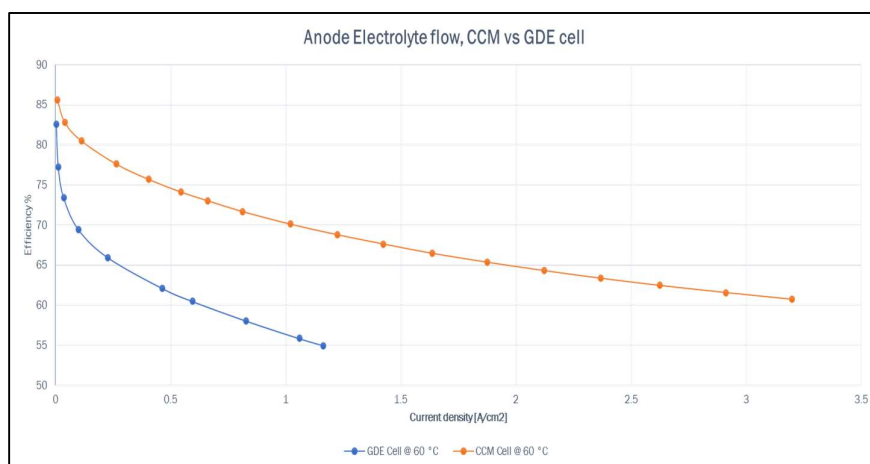


Figure 25. Efficiency comparison between cell #1 (GDE) and cell #3 (CCM)

Finally, the performance of the studied cells is summarized and compared to other results found in the literature in Table 6.

Table 6. Performance of AEMWE cells tested in this work

Anode	Cathode	Membrane and electrolyte	Performance and temperature	Reference
Ni-Alloy	Ni-Alloy	PiperIon A80 80 μ m 1 M KOH	0.1 A/cm ² at 1.79 V (60 °C) 0.464 A/cm ² at 2.0 V (60 °C)	This work
IrRuO _x 3 mg	PtB 3 mg	Pention-75-15CL 30 μ m 1 M KOH	1.224 A/cm ² at 1.81 V (60 °C) 2.912 A/cm ² at 2.02 V (60 °C)	This work
Ni-Foam	Pt/C 0.5 mg/cm ²	PiperIon 80 μ m 1 M KOH	0.3 A/cm ² at 1.8 V (60 °C) 0.62 A/cm ² at 2.0 V (60 °C)	(Caielli et al., 2023)
Fe _x Ni _y OOH-20F	Pt/C	PAP-TP-85 20 μ m Pure water	1020 mA/cm ² at 1.8 V (90 °C)	(Xiao et al., 2021)
IrO ₂	Pt/C	PiperIon TP-85 50 μ m Pure water	1.00 A/cm ² at 2.0 V (65 °C)	(Lindquist et al., 2021)
RP/SP Perovskite LaSr _{2.7} Co _{1.5} Fe _{1.5} O ₁₀	Pt/C	Pention-72-05 50 μ m 6 M KOH	2.01 A/cm ² at 2.00 V (60 °C) 3.00 A/cm ² at 2.19 V (60 °C)	(Tang et al., 2022)

Performance of the components

The performance data, with the exception of the one recovered from cell #2 because no reference electrode data was recorded, was analyzed accordingly to the procedure described in the section *Procedure for calculating the electrode potentials from reference electrode data* in page 23 and the results can be found in Table 7 and Table A 1.

The results from fitting CF and E_{ref} are expressed in (33) and (34). E_{ref} was found to vary between -0.1 and -0.9 V respect to SHE. This can be easily explained with the help of equation (14) that suggests that between pH 0 and 14 a hydrogen reference electrode can vary its potential between 0 and -0.84 V respect to SHE. This further suggests the hypothesis that the pH of the electrolyte in contact with the reference electrode in the cell was changing constantly throughout the experiments. CF values instead leaned towards 0 for cell # 1 and towards 1 for cell # 3, which would support the hypothesis that the parameter is affected by the manner the cell is assembled.

$$-0.1 < E_{ref} < -0.9 \quad (33)$$

$$0 < CF < 1 \quad (34)$$

Table 7. Results from parameter fitting in MATLAB

Cell	Temp [°C]	Ohmic resistance [mΩ/cm ²]	i0 Anode [A/cm ²]	i0 Cathode [A/cm ²]	Anode	Cathode	Membrane
1	30	548.8	1.61E-06	4.85E-06	Ni-Alloy	Ni-Alloy	PiperION A80
1	41	427.8	8.64E-06	2.14E-06	Ni-Alloy	Ni-Alloy	PiperION A80
1	61	363.2	1.62E-05	6.71E-06	Ni-Alloy	Ni-Alloy	PiperION A80
1	74	348.0	5.37E-06	2.75E-05	Ni-Alloy	Ni-Alloy	PiperION A80
3	41	105.6	2.90E-07	9.32E-02	IrRuOx	PtB	Pention-72-15CL 30um
3	61	101.9	4.65E-06	2.44E-02	IrRuOx	PtB	Pention-72-15CL 30um

The fitted ohmic resistances and the HFR readings are plotted in Figure 26a. First, it can be observed that the PiperIon AEM has a much higher ASR compared to Pention AEM, which goes in line with the reduction in thickness from 80 μm to 30 μm. Second, at least for the PiperIon AEM it can be seen clearly how the ASR decreases with increasing temperature in a nonlinear manner, which would agree with the observations in literature that AEM conductivity usually follows an Arrhenius type behavior. Third, for the Pention AEM the fitted ohmic resistances and HFR readings point to similar ASR values, however, this is not the case for PiperIon AEM where they diverge considerably. For the moment no explanation can be formulated for this last point, which could be addressed in future experiments.

The exchange current densities obtained from fitting a Butler-Volmer model for anode and cathode of cell # 1 and for anode of cell # 3 are plotted in Figure 26b. The results for the cell # 3 cathode were not plotted as they are several orders of magnitude higher than the rest of the results and which puts into evidence the superior performance of PtB catalyst over Ni-alloy for

HER. IrRuO_x catalyst and Ni-alloy show similar performance which demonstrates that IrRuO_x is not an outstanding catalyst for OER in alkaline media despite being made from PGM materials. These conclusions are in line with the trends shown by OER and HER catalysts in Table 1 and Table 2.

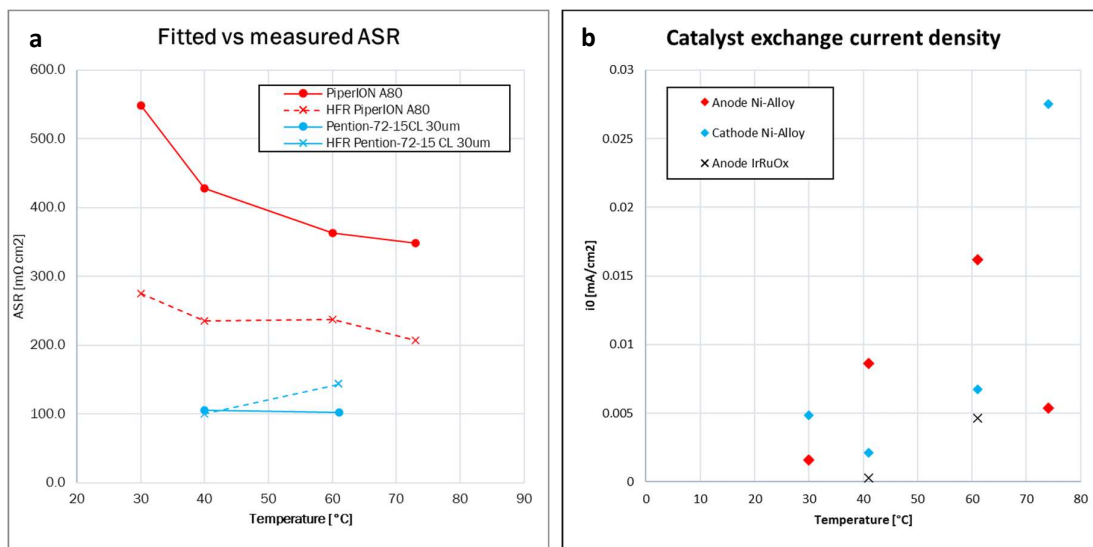


Figure 26. Comparison of (a) Area specific resistances and (b) estimated exchange current densities between cell #1 and #3

An issue arises when trying to use the data to draw further conclusions. This is because there are some inaccuracies and intrinsic errors associated to the methodology that affect the accuracy and exactitude of the results. This can be appreciated in Figure 27b where the cathode overvoltage at very low current densities does not agree with Butler-Volmer behavior despite the good concordance achieved between the final model and the polarization curve (Figure 27a). Additional figures for the rest of the configurations can be found in the appendix.

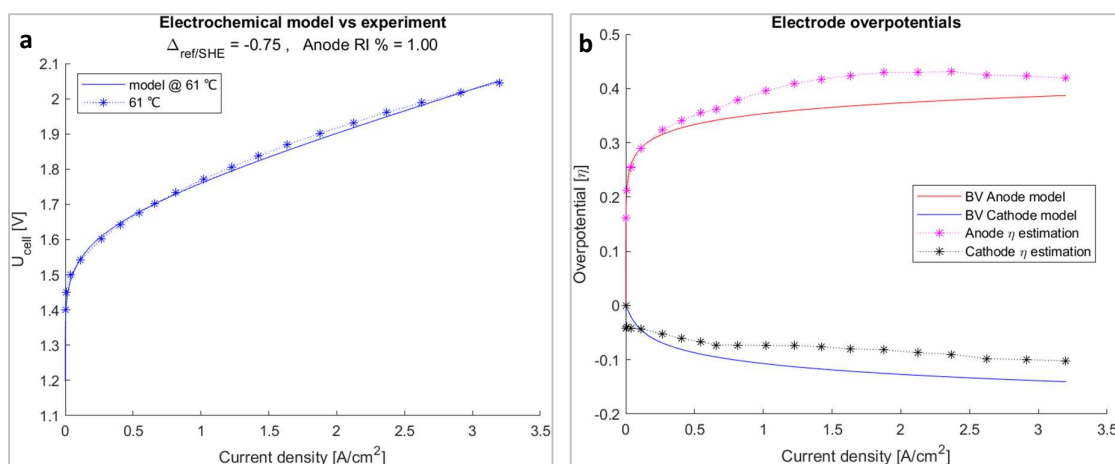


Figure 27. Comparison of (a) measured polarization curve versus electrochemical model and of (b) electrode overvoltage and Butler-Volmer model for cell #3

Nevertheless, to facilitate the discussion of the results with what is found in the literature, the Tafel slope and the overvoltage at 10 mV and 100 mV were calculated for HER and OER and are presented in Table 8 and Table 9. For HER catalysts, performance of the Ni-alloy catalyst

agrees with what was found in the literature for Nickel foam. Performance of PtB looks exceptional, however, the low TS values of just 7 and 3 suggests superb catalyst performance that may not be accurate, a case already explained with the help of Figure 27b. In despite of that, we can still conclude that PtB performance is much superior to that of Ni-Alloy and one reason why cell #3 vastly outperformed cell #1.

Table 8. Estimated performance of HER catalysts used in this work

Cell	T	Catalyst (HER)	Electrolyte	η (mV) at j mA/cm ²	TS (mV/dec)	Ref
1	30	Ni-Alloy	1 M KOH	189 mV @ 10 mA/cm ²	100	*
1	41	Ni-Alloy	1 M KOH	237 mV @ 10 mA/cm ²	90	*
1	61	Ni-Alloy	1 M KOH	194 mV @ 10 mA/cm ²	118	*
1	74	Ni-Alloy	1 M KOH	144 mV @ 10 mA/cm ²	134	*
3	41	PtB	1 M KOH	16 mV @ 10 mA/cm ²	7	*
3	61	PtB	1 M KOH	40 mV @ 10 mA/cm ²	3	*
-	-	NF (Nickel Foam)	1.0 M KOH	180 mV @ 10 mA/cm ²	117	(Zhang et al., 2023)
-	-	Pt/C	0.1 M KOH	125 mV @ 10 mA/cm ²	39	(Lu et al., 2019)
-	-	NS-Ru@NiHO/Ni ₅ P ₄	1.0 M KOH	16 mV @ 10 mA/cm ²	35.2	(K. Wang et al., n.d.)

* This work. These results should not be considered as accurate estimations for catalyst performance.

Regarding OER catalysts, IrRuO_x presents very similar performance to the Ni-alloy catalyst and is in line with other PGM catalysts found in the literature, suggesting that OER performance does not benefit particularly from using PGM materials and opening the door to adopting cheaper and still effective non-PGM catalysts with similar or better performances.

Table 9. Estimated performance of OER catalysts used in this work

Cell	T	Catalyst (OER)	Electrolyte	η (mV) at j mA/cm ²	TS (mV/dec)	Ref
1	30	Ni-Alloy	1 M KOH	315 mV @ 100 mA/cm ²	60	*
1	41	Ni-Alloy	1 M KOH	241 mV @ 100 mA/cm ²	44	*
1	61	Ni-Alloy	1 M KOH	246 mV @ 100 mA/cm ²	59	*
1	74	Ni-Alloy	1 M KOH	282 mV @ 100 mA/cm ²	45	*
3	41	IrRuOx	1 M KOH	318 mV @ 100 mA/cm ²	54	*
3	61	IrRuOx	1 M KOH	280 mV @ 100 mA/cm ²	63	*
-	-	NF (Ni Foam)	1.0 M KOH	382 mV @ 100 mA/cm ²	113	(Zhang et al., 2023)
-	-	Ni(OH) ₂ @NF	1.0 M KOH	387 mV @ 100 mA/cm ²	97	(Zhang et al., 2023)
-	-	IrO ₂	1 M KOH	338 mV @ 10 mA/cm ²	47	(Song & Hu, 2014)

* This work. These results should not be considered as accurate estimations for catalyst performance.

Conclusions

This master thesis is a firsthand experience into assembling and operating a functional AEMWE cell with commercial materials for the first time at LEMTA. Polarization curves were obtained demonstrating the operation of a simple PGM-free water electrolysis cell with Ni-alloy catalyst capable of reaching a current density of 0.464 A/cm^2 at 2.0 V and 60 °C; and it was demonstrated how increasing the temperature increases performance in part thanks to the reduced ASR of the PiperIon AEM. It was also demonstrated for this case that anhydrous cathode operation (electrolyte fed through the anode) can achieve higher performance than anhydrous anode operation (electrolyte fed through the cathode) and how this behavior can be explained thanks to the affinity of OER to the increase in ion-transport pathways and ECSA result of using a supporting liquid electrolyte such as 1 M KOH solution.

Furthermore, polarization curves were also obtained that demonstrate the very respectable performance of a PGM cell with IrRuO_x and PtB catalyst for anode and cathode respectively capable of reaching a current density of 2.91 A/cm^2 at 2.02 V and 60 °C.

By using a Reversible Hydrogen Electrode setup developed at LEMTA, information about catalyst performance was obtained for both cells tested. It is hypothesized that the potential of this reference electrode varies considerably with operating conditions and that the ohmic drop compensation factor for iR-drop correction varies with the cell assembly method. A calculation methodology was created in MATLAB to circumvent these limitations and the results are thus reported for comparison, but with the warning that the amount of error might be high in some cases.

Nevertheless, the results suggest that the PGM catalyst IrRuO_x performance is not superior to Ni-alloy and to other OER catalysts, thus opening the door to the possibility to use other alternative non-PGM catalysts that could show higher performance. On the other hand, PtB had a remarkably good performance, which is in line with the general trend for HER catalyst to perform extremely well with small amounts of PGM metals like Ruthenium and Platinum.

Overall, this master thesis is a steppingstone into developing high performance AEMWE cells and it introduces some key discussions surrounding the effect of material selection and interaction to the cell performance.

Perspectives

In view of the conclusions of this master thesis, there are many roads that can be followed in order to develop high performance AEMWE cells:

- Improve the testing methodology by fixing CF and E_{ref} . CF should equal to 0.5 if careful cell assembly procedures are followed, and for E_{ref} the properties of the electrolyte surrounding the reference electrode should be kept constant, e.g., by feeding to the reference electrode an electrolyte with constant pH value.
- Find out why the ASR measurements from HFR diverged from the fitted results.
- Find an appropriate method to precondition AEMWE cell performance before taking measurements.
- Explore the influence of feeding electrolyte through both electrodes in the whole range of current densities. In this case, attention has to be given to the water balance and electrolyte concentration of the cell.
- Analyze H_2 percentage in O_2 to take into account the crossover effects in the membrane.
- Evaluate different AEMs and different thicknesses since this has a direct effect on cell performance. Evaluate the water transport across these AEMs as this can have a direct effect on electrocatalyst performance in the cathode particularly during anhydrous cathode operation.
- Explore the OER performance of the catalyst layer giving attention to the ion-transport pathways. Gas and charge transport can also be considered. Here there is a huge potential for studying many highly active non-PGM catalysts. Phosphorous and Sulfur Nickel compounds and their combination as well as stainless steel alloys are just some out of many OER electrocatalyst found in the literature review that have high OER catalytic activity.
- Explore the HER performance of the catalyst layer giving attention to the water transport properties of the CL. Water retention in the CL during anhydrous cathode operation has been found to be important for high CL performance in the literature. Additionally, Platinum and Ruthenium on Nickel has been found to produce highly active HER catalysts and it could be interesting to try some of these catalysts in high performing AEMWE cells.

References

- About Montreal Protocol*. (2018, October 29). Ozonation. <http://www.unep.org/ozonation/who-we-are/about-montreal-protocol>
- About the secretariat | UNFCCC*. (n.d.). Retrieved July 10, 2023, from <https://unfccc.int/about-us/about-the-secretariat>
- Aili, D., Kraglund, M. R., Rajappan, S. C., Serhiichuk, D., Xia, Y., Deimede, V., Kallitsis, J., Bae, C., Jannasch, P., Henkensmeier, D., & Jensen, J. O. (2023). Electrode Separators for the Next-Generation Alkaline Water Electrolyzers. *ACS Energy Letters*, *8*(4), 1900–1910. <https://doi.org/10.1021/acsenergylett.3c00185>
- Anantharaj, S., & Noda, S. (2022). iR drop correction in electrocatalysis: Everything one needs to know! *Journal of Materials Chemistry A*, *10*(17), 9348–9354. <https://doi.org/10.1039/D2TA01393B>
- Anantharaj, S., Noda, S., Driess, M., & Menezes, P. W. (2021). The Pitfalls of Using Potentiodynamic Polarization Curves for Tafel Analysis in Electrocatalytic Water Splitting. *ACS Energy Letters*, *6*(4), 1607–1611. <https://doi.org/10.1021/acsenergylett.1c00608>
- Caielli, T., Ferrari, A. R., Bonizzoni, S., Sediva, E., Capri, A., Santoro, M., Gatto, I., Baglio, V., & Mustarelli, P. (2023). Synthesis, characterization and water electrolyzer cell tests of poly(biphenyl piperidinium) Anion exchange membranes. *Journal of Power Sources*, *557*, 232532. <https://doi.org/10.1016/j.jpowsour.2022.232532>
- Cazot, M. (2019). *Development of Analytical Techniques for the Investigation of an Organic Redox Flow Battery using a Segmented Cell* [These de doctorat, Université de Lorraine]. <https://www.theses.fr/2019LORR0116>
- Chatenet, M., Pollet, B. G., Dekel, D. R., Dionigi, F., Deseure, J., Millet, P., Braatz, R. D., Bazant, M. Z., Eikerling, M., Staffell, I., Balcombe, P., Shao-Horn, Y., & Schäfer, H. (2022). Water electrolysis: From textbook knowledge to the latest scientific strategies and industrial developments. *Chemical Society Reviews*, *51*(11), 4583–4762. <https://doi.org/10.1039/D0CS01079K>

- Chen, N., Paek, S. Y., Lee, J. Y., Park, J. H., Lee, S. Y., & Lee, Y. M. (2021). High-performance anion exchange membrane water electrolyzers with a current density of 7.68 A cm⁻² and a durability of 1000 hours. *Energy & Environmental Science*, 14(12), 6338–6348.
<https://doi.org/10.1039/D1EE02642A>
- DAEMONHYC. (n.d.). *Pepr Hydrogène*. Retrieved August 20, 2023, from <https://www.pepr-hydrogene.fr/projets/daemonhyc/>
- Du, N., Roy, C., Peach, R., Turnbull, M., Thiele, S., & Bock, C. (2022). Anion-Exchange Membrane Water Electrolyzers. *Chemical Reviews*, 122(13), 11830–11895.
<https://doi.org/10.1021/acs.chemrev.1c00854>
- Electrolyzers: The tools to turn hydrogen green.* (2023). Chemical & Engineering News.
<https://cen.acs.org/materials/electronic-materials/Electrolyzers-tools-turn-hydrogen-green/101/i21>
- Endrődi, B., Kecsenovity, E., Samu, A., Halmágyi, T., Rojas-Carbonell, S., Wang, L., Yan, Y., & Janáky, C. (2020). High carbonate ion conductance of a robust PiperION membrane allows industrial current density and conversion in a zero-gap carbon dioxide electrolyzer cell. *Energy & Environmental Science*, 13(11), 4098–4105. <https://doi.org/10.1039/D0EE02589E>
- Faqeeh, A. H., & Symes, M. D. (2023). A standard electrolyzer test cell design for evaluating catalysts and cell components for anion exchange membrane water electrolysis. *Electrochimica Acta*, 444, 142030. <https://doi.org/10.1016/j.electacta.2023.142030>
- Fu, C., O'Carroll, T., Shen, S., Luo, L., Zhang, J., Xu, H., & Wu, G. (2023). Metallic-Ir-based anode catalysts in PEM water electrolyzers: Achievements, challenges, and perspectives. *Current Opinion in Electrochemistry*, 38, 101227. <https://doi.org/10.1016/j.coelec.2023.101227>
- Global Hydrogen Review 2022 – Analysis.* (n.d.). IEA. Retrieved July 11, 2023, from <https://www.iea.org/reports/global-hydrogen-review-2022>
- Gong, M., Zhou, W., Tsai, M.-C., Zhou, J., Guan, M., Lin, M.-C., Zhang, B., Hu, Y., Wang, D.-Y., Yang, J., Pennycook, S. J., Hwang, B.-J., & Dai, H. (2014). Nanoscale nickel oxide/nickel heterostructures for active hydrogen evolution electrocatalysis. *Nature Communications*, 5(1), Article 1. <https://doi.org/10.1038/ncomms5695>

- Hua, D., Huang, J., Fabbri, E., Rafique, M., & Song, B. (2023). Development of Anion Exchange Membrane Water Electrolysis and the Associated Challenges: A Review. *ChemElectroChem*, *10*(1), e202200999. <https://doi.org/10.1002/celec.202200999>
- Huang, G., Mandal, M., Peng, X., Yang-Neyerlin, A. C., Pivovar, B. S., Mustain, W. E., & Kohl, P. A. (2019). Composite Poly(norbornene) Anion Conducting Membranes for Achieving Durability, Water Management and High Power (3.4 W/cm²) in Hydrogen/Oxygen Alkaline Fuel Cells. *Journal of The Electrochemical Society*, *166*(10), F637. <https://doi.org/10.1149/2.1301910jes>
- Ito, H., Miyazaki, N., Sugiyama, S., Ishida, M., Nakamura, Y., Iwasaki, S., Hasegawa, Y., & Nakano, A. (2018). Investigations on electrode configurations for anion exchange membrane electrolysis. *Journal of Applied Electrochemistry*, *48*(3), 305–316. <https://doi.org/10.1007/s10800-018-1159-5>
- Javed, H., Zanchi, E., D'Isanto, F., Bert, C., Ferrero, D., Santarelli, M., & Smeacetto, F. (2022). Novel SrO-Containing Glass-Ceramic Sealants for Solid Oxide Electrolysis Cells (SOEC): Their Design and Characterization under Relevant Conditions. *Materials*, *15*(17), Article 17. <https://doi.org/10.3390/ma15175805>
- Kang, S. Y., Park, J. E., Jang, G. Y., Kim, O.-H., Kwon, O. J., Cho, Y.-H., & Sung, Y.-E. (2022). High-performance and durable water electrolysis using a highly conductive and stable anion-exchange membrane. *International Journal of Hydrogen Energy*, *47*(15), 9115–9126. <https://doi.org/10.1016/j.ijhydene.2022.01.002>
- Li, D., Motz, A. R., Bae, C., Fujimoto, C., Yang, G., Zhang, F.-Y., Ayers, K. E., & Kim, Y. S. (2021). Durability of anion exchange membrane water electrolyzers. *Energy & Environmental Science*, *14*(6), 3393–3419. <https://doi.org/10.1039/D0EE04086J>
- Light Bridge. (n.d.). Retrieved July 18, 2023, from <https://lightbridge.co.kr/>
- Lindquist, G. A., Oener, S. Z., Krivina, R., Motz, A. R., Keane, A., Capuano, C., Ayers, K. E., & Boettcher, S. W. (2021). Performance and Durability of Pure-Water-Fed Anion Exchange Membrane Electrolyzers Using Baseline Materials and Operation. *ACS Applied Materials & Interfaces*, *13*(44), 51917–51924. <https://doi.org/10.1021/acsami.1c06053>

- Liu, J., Kang, Z., Li, D., Pak, M., Alia, S. M., Fujimoto, C., Bender, G., Kim, Y. S., & Weber, A. Z. (2021). Elucidating the Role of Hydroxide Electrolyte on Anion-Exchange-Membrane Water Electrolyzer Performance. *Journal of The Electrochemical Society*, *168*(5), 054522. <https://doi.org/10.1149/1945-7111/ac0019>
- Liu, J., & Weber, A. Z. (2022). Ionomer Optimization for Hydroxide-Exchange-Membrane Water Electrolyzers Operated with Distilled Water: A Modeling Study. *Journal of The Electrochemical Society*, *169*(5), 054506. <https://doi.org/10.1149/1945-7111/ac69c4>
- Lu, B., Guo, L., Wu, F., Peng, Y., Lu, J. E., Smart, T. J., Wang, N., Finfrock, Y. Z., Morris, D., Zhang, P., Li, N., Gao, P., Ping, Y., & Chen, S. (2019). Ruthenium atomically dispersed in carbon outperforms platinum toward hydrogen evolution in alkaline media. *Nature Communications*, *10*(1), Article 1. <https://doi.org/10.1038/s41467-019-08419-3>
- Luo, X., Rojas-Carbonell, S., Yan, Y., & Kusoglu, A. (2020). Structure-transport relationships of poly(aryl piperidinium) anion-exchange membranes: Effect of anions and hydration. *Journal of Membrane Science*, *598*, 117680. <https://doi.org/10.1016/j.memsci.2019.117680>
- Martinez-Lazaro, A., Capri, A., Gatto, I., Ledesma-García, J., Rey-Raap, N., Arenillas, A., Espinosa-Lagunes, F. I., Baglio, V., & Arriaga, L. G. (2023). NiFe₂O₄ hierarchical nanoparticles as electrocatalyst for anion exchange membrane water electrolysis. *Journal of Power Sources*, *556*, 232417. <https://doi.org/10.1016/j.jpowsour.2022.232417>
- McCrory, C. C. L., Jung, S., Peters, J. C., & Jaramillo, T. F. (2013). Benchmarking Heterogeneous Electrocatalysts for the Oxygen Evolution Reaction. *Journal of the American Chemical Society*, *135*(45), 16977–16987. <https://doi.org/10.1021/ja407115p>
- Minke, C., Suermann, M., Bensmann, B., & Hanke-Rauschenbach, R. (2021). Is iridium demand a potential bottleneck in the realization of large-scale PEM water electrolysis? *International Journal of Hydrogen Energy*, *46*(46), 23581–23590. <https://doi.org/10.1016/j.ijhydene.2021.04.174>
- Moine, C. (2023, April 21). [Communiqué de presse] Le LEMTA célèbre 50 ans d'expertise au service des enjeux sociétaux et environnementaux liés à l'énergie. LEMTA. <https://lemta.univ->

lorraine.fr/communique-de-presse-le-lemta-celebre-50-ans-dexpertise-au-service-des-enjeux-societaux-et-environnementaux-lies-a-lenergie/

Net Zero by 2050 – Analysis. (n.d.). IEA. Retrieved July 11, 2023, from

<https://www.iea.org/reports/net-zero-by-2050>

N. Shah, P., Park, H., Min Tee, H., Dietrich, C., & A. Kohl, P. (2023). In situ amination of anion conducting solid polymer electrolyte membranes. *Materials Advances*, 4(10), 2322–2331.

<https://doi.org/10.1039/D3MA00115F>

Osmieri, L., He, Y., Chung, H. T., McCool, G., Zulevi, B., Cullen, D. A., & Zelenay, P. (2023). La–Sr–Co oxide catalysts for oxygen evolution reaction in anion exchange membrane water electrolyzer: The role of electrode fabrication on performance and durability. *Journal of Power Sources*, 556, 232484. <https://doi.org/10.1016/j.jpowsour.2022.232484>

Parra-Restrepo, J. (2020). *Caractérisation des hétérogénéités de fonctionnement et de dégradation au sein d'un électrolyseur à membrane échangeuse de protons (PEM)* [Phdthesis, Université de Lorraine]. <https://hal.univ-lorraine.fr/tel-02942062>

Parra-Restrepo, J. (2020). *Caractérisation des hétérogénéités de fonctionnement et de dégradation au sein d'un électrolyseur à membrane échangeuse de protons (PEM)* [Phdthesis, Université de Lorraine]. <https://hal.univ-lorraine.fr/tel-02942062>

Pompili, B., & Le Maire, B. (2020). *Stratégie nationale pour le développement de l'hydrogène décarboné en France*. Ministère de la Transition écologique.

<https://www.ecologie.gouv.fr/sites/default/files/DP%20-%20Strat%C3%A9gie%20nationale%20pour%20le%20d%C3%A9veloppement%20de%20l%27hydrog%C3%A8ne%20d%C3%A9carbon%C3%A9%20en%20France.pdf>

<https://www.ecologie.gouv.fr/sites/default/files/DP%20-%20Strat%C3%A9gie%20nationale%20pour%20le%20d%C3%A9veloppement%20de%20l%27hydrog%C3%A8ne%20d%C3%A9carbon%C3%A9%20en%20France.pdf>

Santoro, C., Lavacchi, A., Mustarelli, P., Di Noto, V., Elbaz, L., Dekel, D. R., & Jaouen, F. (2022).

What is Next in Anion-Exchange Membrane Water Electrolyzers? Bottlenecks, Benefits, and Future. *ChemSusChem*, 15(8), e202200027. <https://doi.org/10.1002/cssc.202200027>

Song, F., & Hu, X. (2014). Exfoliation of layered double hydroxides for enhanced oxygen evolution catalysis. *Nature Communications*, 5(1), Article 1. <https://doi.org/10.1038/ncomms5477>

Tahir, M., Pan, L., Idrees, F., Zhang, X., Wang, L., Zou, J.-J., & Wang, Z. L. (2017). Electrocatalytic oxygen evolution reaction for energy conversion and storage: A comprehensive review. *Nano Energy*, 37, 136–157. <https://doi.org/10.1016/j.nanoen.2017.05.022>

- Tang, J., Xu, X., Tang, T., Zhong, Y., & Shao, Z. (2022). Perovskite-Based Electrocatalysts for Cost-Effective Ultrahigh-Current-Density Water Splitting in Anion Exchange Membrane Electrolyzer Cell. *Small Methods*, 6(11), 2201099. <https://doi.org/10.1002/smt.202201099>
- The Paris Agreement* | UNFCCC. (n.d.). Retrieved July 10, 2023, from <https://unfccc.int/process-and-meetings/the-paris-agreement>
- Todoroki, N., & Wadayama, T. (2019). Heterolayered Ni–Fe Hydroxide/Oxide Nanostructures Generated on a Stainless-Steel Substrate for Efficient Alkaline Water Splitting. *ACS Applied Materials & Interfaces*, 11(47), 44161–44169. <https://doi.org/10.1021/acsami.9b14213>
- Todoroki, N., & Wadayama, T. (2023). Stainless Steel Anode for Alkaline Water Electrolysis: Recent Progress in Active and Durable Surface Catalyst Layer Generation. *Materials Transactions, adyub*, MT-MH2022002. <https://doi.org/10.2320/matertrans.MT-MH2022002>
- Tricker, A. W., Lee, J. K., Shin, J. R., Danilovic, N., Weber, A. Z., & Peng, X. (2023). Design and operating principles for high-performing anion exchange membrane water electrolyzers. *Journal of Power Sources*, 567, 232967. <https://doi.org/10.1016/j.jpowsour.2023.232967>
- United Nations Millennium Development Goals*. (n.d.). United Nations. Retrieved July 10, 2023, from <https://www.un.org/millenniumgoals/>
- Versogen—Our revolutionary membranes offer durability and performance. (n.d.). *Versogen*. Retrieved July 12, 2023, from <https://www.versogen.com/revolutionary-anion-exchange-membranes/>
- Vinodh, R., Kalanur, S. S., Natarajan, S. K., & Pollet, B. G. (2023). Recent Advancements of Polymeric Membranes in Anion Exchange Membrane Water Electrolyzer (AEMWE): A Critical Review. *Polymers*, 15(9), Article 9. <https://doi.org/10.3390/polym15092144>
- Wang, F.-L., Xu, N., Yu, C.-J., Xie, J.-Y., Dong, B., Zhang, X.-Y., Dong, Y.-W., Zhou, Y.-L., & Chai, Y.-M. (2023). Porous heterojunction of Ni₂P/Ni₇S₆ with high crystalline phase and superior conductivity for industrial anion exchange membrane water electrolysis. *Applied Catalysis B: Environmental*, 330, 122633. <https://doi.org/10.1016/j.apcatb.2023.122633>
- Wang, J., Zhao, Y., Setzler, B. P., Rojas-Carbonell, S., Ben Yehuda, C., Amel, A., Page, M., Wang, L., Hu, K., Shi, L., Gottesfeld, S., Xu, B., & Yan, Y. (2019). Poly(aryl piperidinium)

- membranes and ionomers for hydroxide exchange membrane fuel cells. *Nature Energy*, 4(5), Article 5. <https://doi.org/10.1038/s41560-019-0372-8>
- Wang, K., Cao, J., Yang, X., Sang, X., Yao, S., Xiang, R., Yang, B., Li, Z., O'Carroll, T., Zhang, Q., Lei, L., Wu, G., & Hou, Y. (n.d.). Kinetically Accelerating Elementary Steps via Bridged Ru-H State for the Hydrogen-Evolution in Anion-Exchange Membrane Electrolyzer. *Advanced Functional Materials*, n/a(n/a), 2212321. <https://doi.org/10.1002/adfm.202212321>
- Wang, L., Weissbach, T., Reissner, R., Ansar, A., Gago, A. S., Holdcroft, S., & Friedrich, K. A. (2019). High Performance Anion Exchange Membrane Electrolysis Using Plasma-Sprayed, Non-Precious-Metal Electrodes. *ACS Applied Energy Materials*, 2(11), 7903–7912. <https://doi.org/10.1021/acsaem.9b01392>
- Wang, T., Wang, Y., & You, W. (2023). Dithiol cross-linked polynorbornene-based anion-exchange membranes with high hydroxide conductivity and alkaline stability. *Journal of Membrane Science*, 685, 121916. <https://doi.org/10.1016/j.memsci.2023.121916>
- Wang, Z., Chen, K., Han, J., Zhang, X., Wang, B., Du, Q., & Jiao, K. (2023). Anion Exchange Membranes for Fuel Cells: Equilibrium Water Content and Conductivity Characterization. *Advanced Functional Materials*, n/a(n/a), 2303857. <https://doi.org/10.1002/adfm.202303857>
- World Energy Transitions Outlook 1-5C Pathway 2022 edition*. (2022, March 29). <https://www.irena.org/publications/2022/mar/world-energy-transitions-outlook-2022>
- Xiao, J., Oliveira, A. M., Wang, L., Zhao, Y., Wang, T., Wang, J., Setzler, B. P., & Yan, Y. (2021). Water-Fed Hydroxide Exchange Membrane Electrolyzer Enabled by a Fluoride-Incorporated Nickel–Iron Oxyhydroxide Oxygen Evolution Electrode. *ACS Catalysis*, 11(1), 264–270. <https://doi.org/10.1021/acscatal.0c04200>
- Xu, K., Ding, H., Lv, H., Chen, P., Lu, X., Cheng, H., Zhou, T., Liu, S., Wu, X., Wu, C., & Xie, Y. (2016). Dual Electrical-Behavior Regulation on Electrocatalysts Realizing Enhanced Electrochemical Water Oxidation. *Advanced Materials*, 28(17), 3326–3332. <https://doi.org/10.1002/adma.201505732>

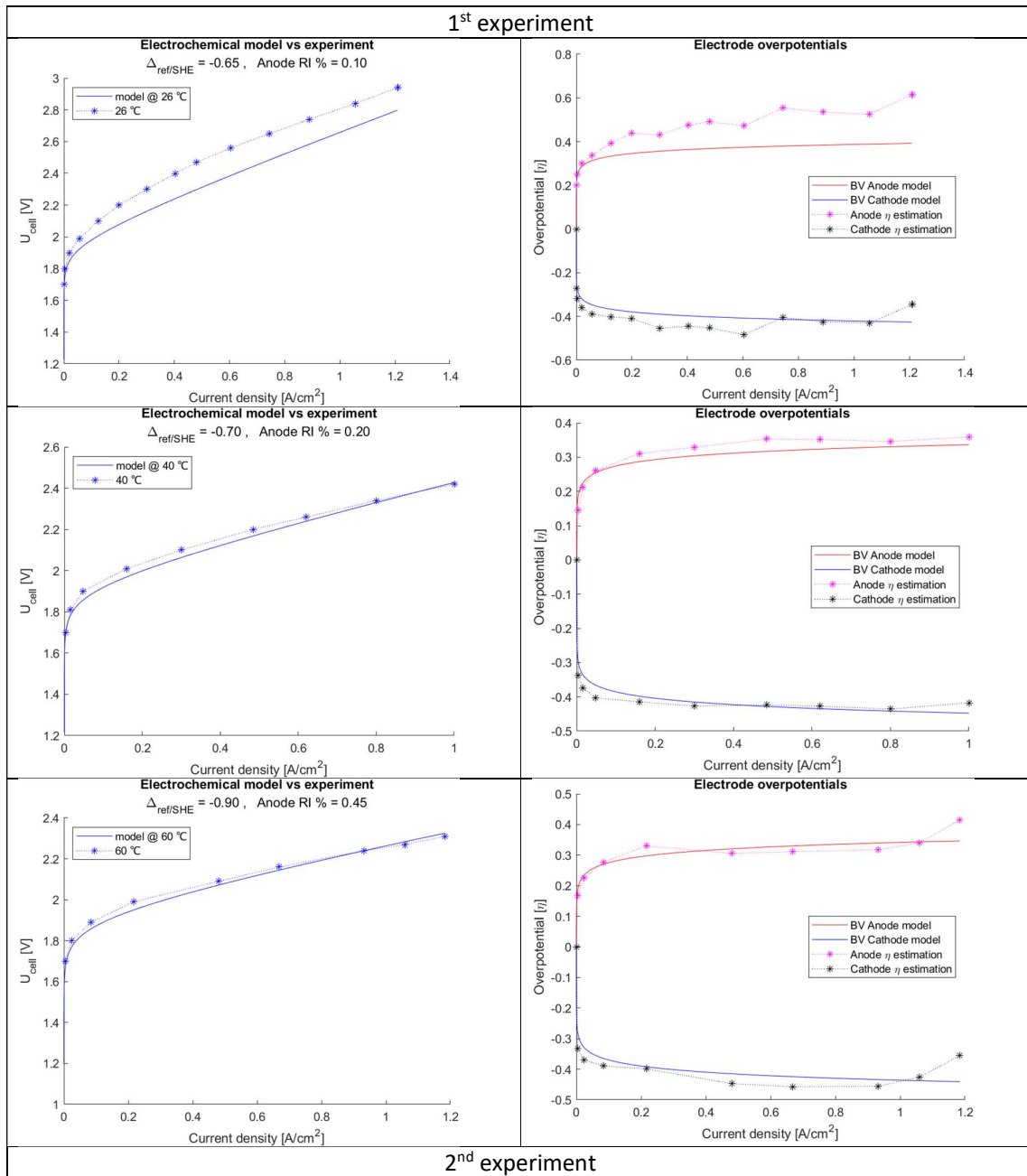
- Zhang, J., Dang, J., Zhu, X., Ma, J., Ouyang, M., & Yang, F. (2023). Ultra-low Pt-loaded catalyst based on nickel mesh for boosting alkaline water electrolysis. *Applied Catalysis B: Environmental*, 325, 122296. <https://doi.org/10.1016/j.apcatb.2022.122296>
- Zheng, Y., Ash, U., Pandey, R. P., Ozioko, A. G., Ponce-González, J., Handl, M., Weissbach, T., Varcoe, J. R., Holdcroft, S., Liberatore, M. W., Hiesgen, R., & Dekel, D. R. (2018). Water Uptake Study of Anion Exchange Membranes. *Macromolecules*, 51(9), 3264–3278. <https://doi.org/10.1021/acs.macromol.8b00034>
- Ziv, N., Mondal, A. N., Weissbach, T., Holdcroft, S., & Dekel, D. R. (2019). Effect of CO₂ on the properties of anion exchange membranes for fuel cell applications. *Journal of Membrane Science*, 586, 140–150. <https://doi.org/10.1016/j.memsci.2019.05.053>

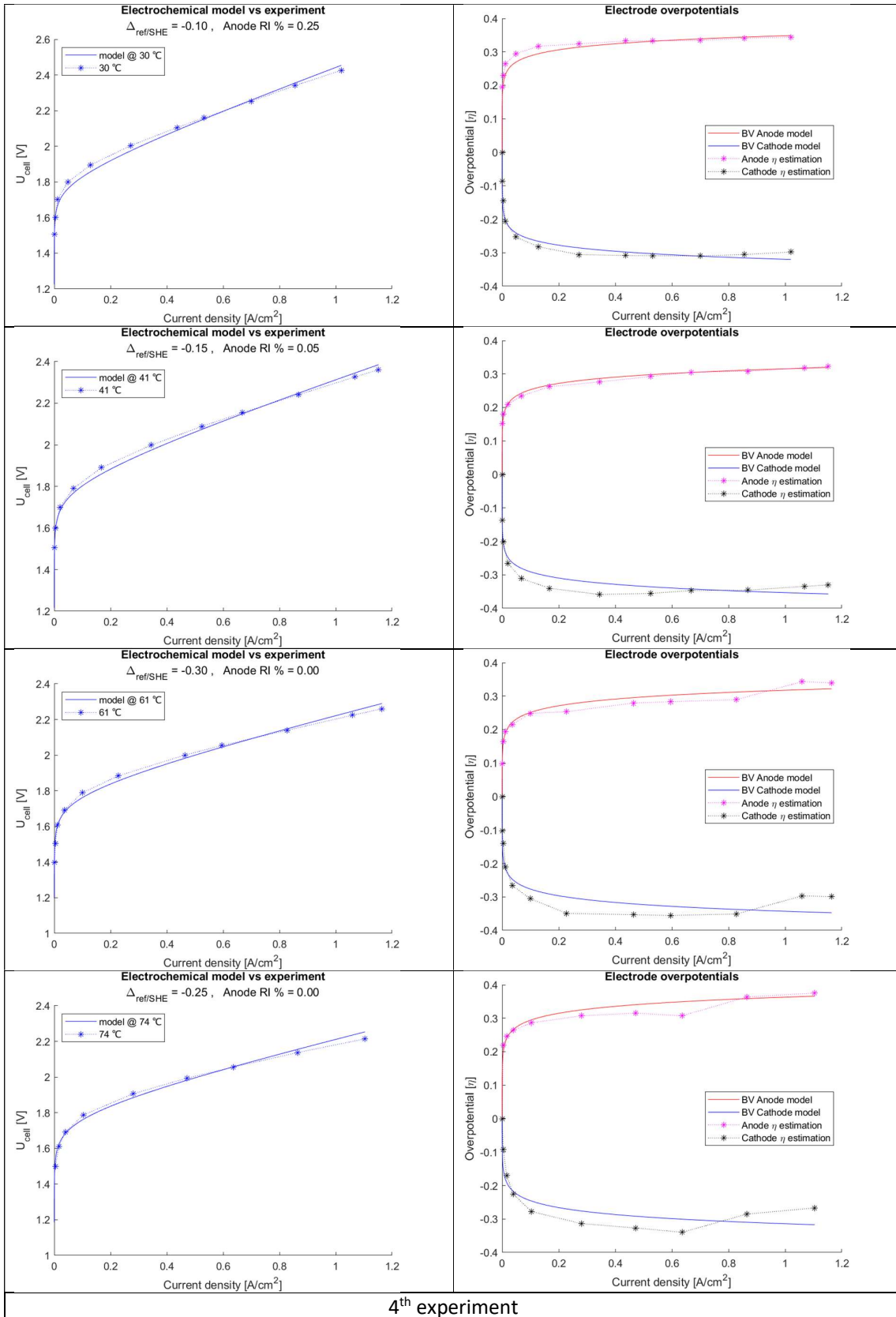
Appendix

Table A 1. Electrochemical and fitting parameters for the cells studied in this work

Exp	temp	R ohmic	i0 anode	i0 cathode	CF	dpp ref_SHE	sse el_model	sse electrodes	ts anode	ts cathode	eta_100 anode	eta_10 cathode
1	26	0.6216	2.98E-07	8.22E-08	0.1	-0.65	0.4523	0.3200	75	-62	355	-343
1	40	0.4275	3.87E-06	6.23E-08	0.2	-0.7	0.0071	0.0119	108	-60	296	-362
1	60	0.2874	6.80E-06	2.55E-07	0.45	-0.9	0.0063	0.0224	82	-44	280	-350
2	30	0.5488	1.61E-06	4.85E-06	0.25	-0.1	0.0849	0.0511	60	-100	315	-189
2	41	0.4278	8.64E-06	2.14E-06	0.05	-0.15	0.0875	0.0477	44	-90	241	-237
2	61	0.3632	1.62E-05	6.71E-06	0	-0.3	0.0452	0.0345	59	-118	246	-194
2	74	0.3480	5.37E-06	2.75E-05	0	-0.25	0.0044	0.0155	45	-134	282	-144
4	41	0.1056	2.90E-07	9.32E-02	0.85	-0.7	0.1138	0.2214	54	-7	318	-16
4	61	0.1019	4.65E-06	2.44E-02	1	-0.75	0.0443	0.0731	63	-3	280	-40

Table A 2. Results of parameter fitting for each set of data





4th experiment

